ADDIS ABABA UNIVERSITY
ADDIS ABABA INSTITUTE OF TECHNOLOGY (AAIT)
SCHOOL OF CIVIL AND ENVIRONMENTAL ENGINEERING
GEODESY AND GEOMATICS PROGRAM

ASSESSMENT OF LAND USE AND LAND COVER CHANGE AND ITS IMPACT ON LAND SURFACE TEMPERATURE USING REMOTELY SENSED DATA: IN AND AROUND GONDAR TOWN, ETHIOPIA

BY: FREW FENTAHUN

ADVISOR: DR. ERMIAS TEFERI

A THESIS SUBMITTED TO

THE SCHOOL OF CIVIL AND ENVIRONMENTAL ENGINEERING, ADDIS ABABA UNIVERSITY IN PARTIAL FULFILLMENT OF THE REQUIREMENTS FOR THE DEGREE OF MASTER OF SCIENCE IN GEODESY AND GEOMATICS PROGRAM (SPECIALIZED IN GEOMATICS)

ADDIS ABABA UNIVERSITY

AUGUST 2020

Approval sheet

Addis Ababa University

School of Graduate Studies

This is to certify the thesis prepared by **FREW FENTAHUN ENYEW**, entitled**: "Assessment of Land Use and Land Cover Change and its impact on LST Using Remotely Sensed Data: In and Around Gondar Town, Ethiopia"** is submitted in partial fulfillment of the requirements for the degree of Masters of Science in Geodesy and Geomatics specialized in Geomatics fulfills the regulations of the University and meets the accepted standards with regards to the originality and quality.

Board of examiners committee:

Dr. Ermias Teferi	_____	_____/_____/_____
Advisor	Signature	Date
Dr. Berhan Gessesse	_____	_____/_____/_____
Internal Examiner	Signature	Date
Dr. Worku Zewdie	_____	_____/_____/_____
External Examiner	Signature	Date
Dr. Ing. Mebruk Mohammed	_____	_____/____/_____
Chairman	Signature	Date

Acknowledgments

First and foremost, I would like to thank the “Almighty God” who gives me strength, patience, and trust to complete my study fruitfully. Then, I wish to explicit my deepest and genuine gratitude to my advisor Dr. Ermias Teferi, who helped me from the starting of the research to its completion and for sharing his constructive comments, scientific guidance, and invaluable input throughout this study.

I would like to extend my deepest gratitude to Dr. Aramde Fetene, Mr. Abubeker Mohamod, Mr. Manaye Tamrie, and Mr.Nigus Adane for his constructive advice, professional comments, and support. I appreciate their constructive comments and provided input in this thesis.

I wish to explicit my genuine thanks to Debre Markos University for sponsoring me for this study.

Further, I have a great appreciation to acknowledge the Central Statistical Agency and Ethiopian Meteorology Agency for providing me the necessary data and information to carry out this study.

Lastly but not the list, I would like to extend my thankfulness to my family for their continuous support. Special thanks go to my beloved wife Marta Nigusie. I appreciate her strength to advice, support, encouragement, and love. And I want to recognize all of those people who were my teachers, friends, and others, who helped me, to begin this long journey. Their names are too plentiful to list, but many of them encouraged me to learn and upgrade.

Table of Contents

List of Tables

List of Figures

List of Annex

Acronyms and Abbreviations

AVHRR	Advanced Very High-Resolution Radiometer
CSA	Central Statistics Agency
DN	Digital Number
ERDAS	Earth Resources Data Analysis System
ETM+	Enhanced Thematic Mapper plus
FAO	Food and Agriculture Organization
GIS	Geographical information system
GPS	Global position system
LP DAAC	Land Processes Distributed Active Archive Center
LSE	Land Surface Emissivity
LST	Landsat Surface Temperature
LULC	Land use and Landcover
MLC	Maximum Likelihood Classification
MODIS	Moderate Resolution Imaging Spectroradiometer
MS	Multi scanner
NASA	National Aeronautical and Space Administration
NDBI	Normalized Difference Built-up Index
NDVI	Normalized Difference Vegetation Index
NOAA	National Oceanic and Atmospheric Administration
OLI	Operational Landsat Imagery
RS	Remote sensing
SWA	Split Window Algorithm
TB	Brightness Temperature

TIRS	Thermal Infrared Sensor
TM	Thematic Mapper
UN	United Nation
UNEPA	United States Environmental Protection Agency
USGS	United States Geology Survey

Abstract

Urban areas are the most dynamic regions in the world which always have a rapid change in both demographic and spatial dimensions. Urbanization is the main cause of global climate change and currently, it is a rising trend globally in general and in Ethiopia in particular. It has a significant influence on land use by substituting areas of natural resources and vegetation with impervious surfaces like built-up asphalt road and parking lots; which in turn increases the LST. The objective of the study was to assess urbanization/LULC and its impacts on LST in urban areas through taking in and around Gondar town. Supervised classification with maximum likelihood algorithm was used to assess the LULC changes and the split-window algorithm was used to extract LST from Landsat imageries which were acquired from 1988, 2002, and 2018 of the same seasons and MODIS LST was used to validate land surface temperature that was derived from Landsat thermal bands. Pearson correlation was used to analyze the relationship between LST and LULC indices (NDVI and NDBI). The results show that there is a significant change in LULC especially the built-up area of the study area which becomes more than triple over the study period from 2.85% - 12.82%. However, Vegetation areas are decreased from 18.78% to 11.4 % from 1988 to 2018. This implies that the areas covered by natural resources and vegetation are replaced with man-made features. Agricultural and bare land areas are also slightly decreased through the study period. This study shows that the LST of Gondar town ranges from 13.44 ℃to 41.32 ℃ from 1988-2018. LST has a positive relationship with NDBI and a negative association between NDVI. Vegetated land and water bodies have low LST. However, most of the agricultural land, bare land, and central parts of Gondar town have high LST. There was a LULC change in Gondar town and it causes an increase in LST from 1988-2018. Therefore, the concerned body should have better environmental management strategies and thermal refreshing mechanisms.

Keywords: Gondar town, LULC, Land Surface Temperature, SWA, and remote sensing

CHAPTER ONE

1. INTRODUCTION

1.1. Background of the study

According to the UN (2014), urbanization is a process whereby the population migrates from the countryside to city areas and from city to city areas, enabling cities and towns to grow. It can be also defined as the progressive increase in the number of societies living in cities. Urban areas are the most dynamic regions in the world. Always, there is a rapid change in both demographic and spatial dimensions with serving as the social and economic centers of our modern life (Galeon, 2009). In the next 20 years, the population of African towns will be more than double and their spatial extent could be more than triple (Lamson-hall et al., 2015).

Thus, such fast human population progress in the city area has been increasing LULC changes worldwide from time to time in quantity and spatial extent (Hansen *et al*., 2013, Defries *et al*., 2004, Lambin *et al*., 2001). Due to the population increase, the need for resource utilization increases proportionally and puts pressure on natural resources and damages them. Besides, the land has been endlessly and extremely reducing due to anthropogenic factors (Brink *et al*., 2014, Niamir-Fuller *et al*., 2012). It has a substantial influence on land use by substituting areas of natural resources and vegetation with residential and commercial areas and their related infrastructure (Bekele, 2005).

In most Eastern African countries, LULC change has been occurred due to the increase of both the human and cattle populations (Pomeroy *et al*., 2003). Overpopulation damages land through overutilizing of land for agricultural activities such as cropping and grazing. This leads to change land covered by natural vegetation is transformed into the town area and built-up lands, farmlands, and grazing lands. This causes soil erosion, deforestation, land degradation, and loss of biodiversity, (Maitima *et al*., 2009), as well as climate change that leads to global warming.

Ethiopia also one of East Africa countries, where the problem of LULC change is very high and it has been increasing from time to time. This is mostly due to population growth (Hurni *et al*., 2005) and insights of local communities towards sustainable land management (Belay *et al*.,

2014). Furthermore, the country is exposed to surface flooding, runoff, and sedimentation (Hurni *et al*., 2005). The land is very dynamic in all parts of the country. Particularly in Amhara National Regional State, the problem is very high as the land is not adequate to support the people of the region. Because of this condition, forest, shrubland, bushland, and grasslands have been heavily degraded due to obtaining additional land for settlement, farmland, and grazing land. This land degradation in turn resulted in the rising of LST (Bekele, 2005).

An increase in LST is major environmental problems in both rural and town areas due to the conversion of vegetated surfaces into built-up, bare, and agricultural land. LST is a significant variable for environmental studies and measured using thermal bands of different sensors such as MODIS, Landsat-5 thematic mapper, Landsat-7 enhanced thematic mapper plus, and Landsat-8 Thermal infrared sensor (Gebrekidan, 2016). LST can be defined in remote sensing language as the surface radiometric temperatures emitted by the land surfaces and observed by a sensor at instance viewing angles (Prata *et al*., 1995). It is also defined as the temperature of the earth's surface phenomena and the feeling of how much hot the surface of the earth is derived from direct measurements or from remotely sensed information (Kayet *et al*., 2016).

Therefore, LST assisted by thermal bands of Landsat imageries to investigate the relationship between town thermal patterns and LULC, is a major application of remote sensing in town climate studies, as it helps land use and occupation planning. Thus, this study goals to assess the relationship between urban LULC change and LST. Therefore, it is useful input to predict future land warming and to provide practical information for urban planners, natural resources managers, and environmental experts to manage natural landscapes to be sustainable and healthy.

1.2. Statement of the problem

Urbanization is currently an increasing trend globally, particularly at an alarming rate in developing countries like Africa and Asia. Urbanization in Africa is continuously increasing from 2010-2015 and is predicted to be 56% with an annual increment of 1.1%. In the same way, Ethiopia is found in eastern Africa where urban dwellers have been increasing from 19% in 2014 and are expected to be 38% in 2050. The urban growth rate of Ethiopia from 2010-2015 was 2.3% (UN, 2014). It has a substantial influence on LULC by substituting areas of natural

resources and vegetation with residential and commercial areas and their related infrastructure (Bekele, 2005).

Since Gondar town found in Ethiopia, the pattern of LULC has been changing from time to time due to rapid urbanization (increase in the number of people living in town areas). LULC change particularly rapid increase built-up and impervious surfaces such as asphalt and parking lots by depleting of other land covers like vegetation and agricultural land of the surrounding areas increase solar radiation absorption and thermal conductivity. This increase of radiation on the biophysical surface material makes the town warmer and warmer from time to time. These are the main cause of LST variation, which is very essential to the study of town climates (Voogt and Oke, 2003).

Such an increment of LST in the town area increase the demands for air conditioning, and consumptions of both water and electricity, and may change rainfall patterns that lead to alterations to biotic communities (Abel, 2018). An excess amount of heat may also affect the comfort of urban dwellers and lead to greater health risks (Rinner and Hussain, 2011). LST also modifies the air temperature of the atmospheric border layer and is a key component in the surface energy balance of the town. Changes in urban LST have their effects on local weather and climate of Gondar town. These changes also have negative impacts on landscape aesthetics, energy efficiency, human health, and quality of living in a town environment (Yue *et al*., 2007).

Evaluating the land use practice and the land cover type and its effects are very essential to investigate LST and monitoring and determining climate change for sustainable environmental resource management. This is because LULC is the most important variable of global changes that disturb ecological systems. As a result, the characteristics of LULC and its patterns have imperative effects on climate, biogeochemistry, hydrology, the diversity and abundance of terrestrial species, and peoples' livelihoods (Eckert *et al*., 2017).

Therefore, investigate urban LULC change and LST using remotely sensed data is very essential to alleviate these problems and forward better solutions. This is because remote sensing is very capable to retrieve LST, land surface emissivity, NDBI, and NDVI using different algorithms and analyze the association between these parameters as well as the impacts of urban LULC

change on the earth's ecosystem. So, by doing this research, it is possible to show the degree to which the environment and climate in Gondar town have changed.

1.3. Objectives of the study

1.3.1. General objective

The general objective of this study is to assess the LULC changes in and around Gondar town and its impact on the distribution and changes of LST from 1988 to 2018 using remotely sensed data.

1.3.2. Specific objectives

- To investigate urban LULC changes of Gondar town from 1988 - 2018.
- To assess the Spatio-temporal distribution of land surface temperature in and around Gondar town.
- To examine the association of LULC indices with a land surface temperature in and around Gondar town.
- To identify land surface temperature changes on each LULC type from 1988 - 2018.

1.4. Research question

This study answers the following questions:

- What are the various classes of LULC in and around Gondar town through the study period (1988, 2002, and 2018)?
- What is the rate of change in LULC in and around Gondar town?
- What is the magnitude of surface temperature in Gondar town through the study period (1988, 2002, and 2018)?
- What is the average LST value of each LULC type within the study period?
- What type of correlation exists between LULC indices (NDVI and NDBI) and LST?

1.5. Scope of the study

The focus of the study is Gondar town in the Amhara National Regional State of Ethiopia. This area is chosen because Gondar town is a growing town and there is an expansion of built-up

areas and impervious surfaces by depleting of other LULC types. Consequently, the LST of the town has been rising from time to time. However, the increase of LST is not investigated by research rather than the perception of local communities. Therefore, this study was conducted to know and compute the trend of LULC change, to know the association of LST with urban LULC, and to analyze the impact of LULC dynamics on LST change. For each LULC class, the LST values assessed and LULC classification should be supported by field verification. Increasing LST leads to an environmental problem such as climate change and seasonal fluctuation. Unless land for built-up, bare land and agriculture is properly managed, it can affect the environment. Therefore, to overcome this problem, the present study was contributed to decision-makers, urban planners, environmental management experts as information, and identifying different LULC classes and changes.

1.6. Significance of the study

As Gondar is fast growing and the economic center of north Gondar in the Amhara National Regional State, the pattern and the type of LULC changes have been proportionally rapid. These types of changes in landscape affect LULC of the town and cause LST to increase; and therefore, they need different LULC planning, and LST mitigation, adaptation strategies, and options. To see the change in LST, the types of LULC and their changes have to primarily analyze through applying change detection analysis. Here, satellite data and remote sensing techniques play a great role. Thus, preparing an up-to-date LULC map helps for proper land use planning and environmental protection. The result of this study can be used in decision making and planning about mitigation measures of the impacts of LULC change. Furthermore, the study is important to analyze spatial and temporal variations of LST, how it may change, and why it changes; examine the association of LST with each LULC and indices (NDVI and NDBI). Information obtained from this study may also be used for spatial planning especially land management and hydrology. Therefore, the output of the study serves as an input for researchers, environmental and hydrologic experts, policymakers, and other stakeholders.

1.7. Structure of the thesis

The first chapter contains an introduction, statement of the problem, objectives of the study, research questions, scope of the study, and significance of the study while chapter two focused

on the literature review related to this study. The second section includes a brief understanding of LULC changes, LST, NDBI, SWA, NDVI, and remote sensing. The third chapter illustrates the general methodology including, the data used in the study, and a comprehensive explanation of Gondar town. Chapter four describes the results and discussion, which presents the detailed results from image classification and collected data. In this chapter, LULC maps generated using maximum likelihood classification, LST, NDBI, zones of LST map, and NDVI results are presented. Additionally, change analysis of LULC and LST, a spatial map was prepared for the comparison of changes in each year, and the Pearson correlations between LST with NDBI and NDVI are presented. Finally, chapter five presents conclusions and recommendations. In this part, a key point of the study and critical points that need further treatment has been forwarded as a recommendation for decision-makers and future investigation.

CHAPTER TWO

2. LITERATURE REVIEW

Under this chapter, the basic concepts and meaning of LULC, LST, NDVI, remote sensing, NDBI, and Split window algorithm. Additionally, it tries to explore the findings of relevant studies that have been studied previously in a different area.

2.1. Concept of Land use and Land cover change

The earth's surface has been changed considerably in the past decades, mostly by human-induced factors such as deforestation, agricultural activities, and urbanization. Land is the ultimate resource of the biosphere and mostly the definition of LULC has been used as one indifferent condition. However, these two words have different meanings. Land cover represents the biophysical state of the earth's surface, such as water bodies, vegetation, soil, and hard surfaces. Whereas, land use represents the utilization of the land by human activities such as settlements, agriculture, forestry, and changing land surface processes including biogeochemistry, hydrology, and biodiversity (Di Gregorio and Jansen, 2000). In this context, variation in the surface component of the landscape is only considered to occur if the surface has a different appearance when viewed on at least two successive occasions (Lemlem, 2007). According to FAO (1999), the definition of land use is the measures, activities, and inputs people assume in a certain land cover type to create change or to maintain it. Change in LULC is occurred by an adverse socio-ecological response that comes from a rigorous degradation in ecosystem services (Lambin and Meyfroidt, 2011).

Land cover change refers to the conversion of one land cover category to a new cover category or modification of one land cover category. Whereas, land-use change refers to a conversion of land use due to human activities for different purposes such as for settlement, infrastructural development, agriculture, and recreational use. Another definition of LULC change is the human modification and conversion of the earth's terrestrial surface. Modification happens when the change affects only the properties of the land cover without causing a complete shift from one LULC category to the other or completely replaced by another (Lambin *et al*., 2003).

2.2. The Driving forces of urban Land use and Land cover Change

Land use and land cover changes are influenced by different factors related to human population growth, economic development, and technology changes. Land cover changes are a conversion of land cover from one category to another and modification of the conditions within a category. Whereas land-use change occurs when land experts decide that an alteration to another land utilization category is desirable (Meyer and Turner, 1992). According to USEPA (2004), the general causes of LULC changes are:

- Natural procedures, such as climate and atmospheric variations, wildfire, and pest infestation.
- The direct effect of human activity such as road and illegal house construction and deforestation.
- An indirect effect of human activity such as water diversion leading to the lowering of the water table and contamination of groundwater.

Human-induced (Anthropogenic) factors are the major driving forces of land use and land cover changes (Niamir-Fuller et al., 2012) even though there is also a contribution from the natural processes. Nowadays, the human-related causes of LULC changes are very serious (Agarwal et al., 2002). There are several types of anthropogenic problems for LULC changes. Urban expansion due to rapid population growth is one factor for LULC change subsequently it brings a dramatic change of landscape patterns and types. These changes have been changing the availability of different biophysical resources and lead to decreased availability of different products and services for humans, livestock, and damage to the environment. Therefore, urban expansion in and around urban areas has great impacts on the environment. For example, it causes an increase in the temperature of urban areas (Qijiao and Zhixiang, 2015).

Additionally, population growth decreases forest areas because they use it as fuelwood and timber, and woodlands for grazing by their livestock. People are the most important natural resources which are mutually interrelated and interdependent for their sustainable development. However, Land use reflects the significance of land as a basic and limited resource for most human activities such as forestry, agriculture, industry, energy production, recreation, settlement, and water catchment and storage. During the past three centuries, the extent of earth cultivated

land has grown by more than 45% increase from 2.65 million km² to 15 million km² and at the same time, other natural resources such as forest have been shrinking due to agricultural land expansion and urbanization (Santa, 2011). The percentage of deforestation is high in many developing countries associated with population growth and poverty (Mather and Needle, 2000).

Desertification is also another effect of unsafe land use and land cover change. It escalates the concentration of carbon-di-oxide (co_2) in the atmosphere. Therefore, occurrences of forest fire-related to LULC degradation rises the emission of toxic gasses such as carbon monoxide (co) and nitric oxide which change the chemistry of the atmosphere causing air pollution, affecting energy balance and climate and global warming (Peter, 1994). Land use and land cover change have impacts on hydrology. It changes the quality of water and water flows, causing surface water pollution, depletion of groundwater aquifers. Land use and land cover changes also increase the frequency and severity of flooding which is due to continuous and serious deforestation (Meyer and Turner, 1992).

In general, land use and land cover changes have become major problems for the world, and it is a significant driving agent of global environmental changes (FAO, 1999). Such a large-scale land-use class change through the increase of agricultural land in a rural area, deforestation, urbanization, and other natural phenomena and human activities are inducing changes in global systems and cycles. However, the major change in land-use, historically, has been the worldwide increase in agricultural land (Houghton, 1994). Climate change is the long term or permanent shift in the climate of the area. Some of the indications for climate change include an increased frequency of the occurrence of drought, global temperature rise, tropical cyclones, flood, and reduced annual rainfall reduction in glacial cover over a mountain and rising sea levels (Mengistu, 2008).

These, human and natural systems in all geographic scales are affected by dynamic processes due to urban change especially the great global increase of urban population and urbanized areas (Brockerhoff, 2000). The skill to monitor urban LULC changes is highly required by local communities and policy decision-makers. Due to the increased availability and improved quality of multi spatial-temporal data and new analytical techniques, nowadays it is possible to monitor urban LULC changes and urban sprawl in a well-timed and in economical way (Yang *et al*.,

2003). Therefore, the use of remotely sensed data is mandatory for regional planning and urban ecology.

2.3. Land Surface Temperature and its Algorithm

According to Prata et al., (1995) and Schmugge et al., (1998), LST is the surface radiometric temperature corresponding to the direct field of view of the sensor. It is also defined as the temperature emitted by the surface and measured in kelvin (Kayet et al., 2016). Additionally, LST is the temperature measured at the Earth's surface and is regarded as its skin temperature (Dash et al., 2002). LST is the main parameter for various environmental models, such as energy and water exchange between atmosphere and surface (Yuan and Bauer, 2007), numerical weather prediction, global ocean circulation, and climatic variability. It indicates the collective result of all energy interchange processes between the atmosphere and the land surface (Voogt and Oke, 2003). Thus, LST is a basic requirement for model validation or model constraining in surface energy and water budget modeling on different scales (Kalma *et al.*, 2008, Kustas and Anderson, 2009). It works as a metric for soil moistness and vegetation intensities in ecological and hydrological modeling and environmental monitoring (Kustas and Anderson, 2009). Further, LST has been used in the area of thermal errors and high-temperature occurrence detection (Sobrino *et al*., 2009). Land surface temperature is also useful to predict the energy and water interactions between land surface and atmosphere, which plays a significant role in human-environment interactions (Qijiao and Zhixiang, 2015).

Additionally, LST is mostly used in urban climate studies to determine the surface of urban heat island and to investigate its relationship with urban LULC and air temperature variability as well as for surface-atmosphere interaction processes in urban environments(Voogt and Oke, 2003, Weng, 2009). Therefore, LST can be easily derived from satellite data (Lazzarini *et al*., 2013, Li *et al*., 2013), such as Landsat, NOAA-AVHRR, and MODIS. 'For a given sensor viewing direction, LST depends on the distribution of temperature and emissivity within a pixel and the spectral channel of measurement' (Becker and Li, 1995). To acquire LST from satellite images, the atmospheric, angular, and emissivity must be corrected. The main effects of the atmosphere are absorption, upward atmospheric emission, and downward atmospheric irradiance reflected from the surface. Various atmospheric correction methods have been established based on sensor

characteristics. However, the split-window algorithm is commonly used for retrieving LST in Landsat 8.

2.3.1. Split-window algorithm

Becker and Li, (1990), and Price, (1984) describe a split-window algorithm is used for the sensor which has more than one channels, in which radiance differences are detected by each atmospheric window of the respective thermal infrared channel. This technique uses differential absorption between two channels within one atmospheric window to avoid the atmospheric influence and determines the temperature at the sensor using a linear combination of two brightness temperatures (Dash *et al*., 2002). For example in Landsat-8 (Du et al., 2014, Rozenstein et al., 2014) and NOAA-AVHRR (Qin *et al*., 2001). The algorithm uses the LSE values in both thermal infrared channels for calculation of LST (Jin *et al*., 2015).

2.4. Normalized Difference Vegetation Index

The normalized difference vegetation index is an index based on the spectral reflectance of the ground surface feature. Each feature has its characteristic reflectance varying according to the wavelength. NDVI can be developed using near-infrared and red bands of the satellite data and value ranges between -1 to +1. A higher value of NDVI which is close to 1 indicates the presence of healthy vegetation in the area while it's a lower value (-1) is the indicator of the absence of vegetation. Hence, the NDVI is very crucial induces for assessing the health of vegetation, the greenness of the earth's surface, crop monitoring and yield forecasting, and forest cover assessment and deforestation and desertification. NDVI is very essential for analyzing and mapping LULC (Friedl *et al*., 2002). Furthermore, NDVI is very essential for analyzing the urban green environment and urban climate since it indicates the level of dryness and warmness of the area.

2.5. Normalized Difference Built-up Index

The normalized difference built-up index is useful for mapping of urban built-up areas using remotely sensed data. It is used to identify the extent and density of imperviousness surfaces like asphalt road, parking lots, built-up areas, and map these areas (Zha et al., 2003 and Malik et al. 2019). These areas have higher reflectance in the short-wave infrared region than that of the

near-infrared one (Alhawiti and Mitsova, 2016). NDBI can be developed using short wave and near-infrared bands of the remote sensing data and value range between -1 to +1. A higher value of NDBI which is close to 1 indicates the presence of built-up in the area while it's a lower value (-1) is the indicator of the vegetation or absence of built-up surfaces in the area.

2.6. The Significance of Remote Sensing for LULC and LST Analysis

The land is becoming degraded and the pattern and types of land cover are changed in the world. Therefore, the ways of analyzing LULC change occur at different times and places are very essential for sustainable land management and economic development. Furthermore, assessing and mapping the consequences of LULC change and the possible solution is very significant. Monitoring temporal LULC changes are also very important for environmental management. In this regard, remote sensing has been playing a crucial role in providing satellite imageries to assess natural resources and monitor environmental changes. Landsat is one example of satellites that providing synoptic, repetitive, and global coverage data freely since 1972. Landsat imageries have been used for various terrestrial applications. Therefore, Remote Sensing allows analyzing LULC change dynamics using a time series of remotely sensed data by integrating it with socio-economic or biophysical data. Remote sensing is also efficient in land-cover mapping, detecting and monitoring land-cover change over time and space, identifying land use attributes, and land cover change hot spots (Abate, 2011, Abbas *et al*., 2010, Gashaw *et al.*, 2014). Nowadays, the level of technology advanced has a great role to conduct land cover change detection analysis and to predict future scenarios with low data cost, availability of historic spatio-temporal data, and high-resolution satellite images (Agarwal *et al*., 2000).

Moreover, LST and NDVI can be easily computed by using satellite data specifically thermal remote sensing is very crucial for assessing and measuring urban thermal environment (Sun *et al*., 2012). It also provides a tool for analyzing thermal variation measurements of physical, environmental, and socioeconomic variables in urban settings (Small, 2004). Remote sensing data is also significant for analyzing the relationship of LULC change with LST, NDBI, and NDVI.

CHAPTER THREE

3. MATERIAL AND METHOD

The geographical location, population, topography, and climate (temperature and rainfall) of Gondar town were described. The category of data that were used for this study and their sources, the methods of data processing such as layer stack, sub-setting, digital image processing. Multispectral radiometric correction, image classification, accuracy assessment, change detection analysis, and the method used to calculate NDVI, NDBI, and LST were included in this chapter. Additionally, the methods of analysis (zonal statistics and Pearson correlation coefficient) used in this study also a part of this chapter. From these zonal statistics used to determine the value for each LULC class and the Pearson correlation coefficient was used to analyze the association between LST with LULC indices (NDVI and NDBI).

3.1. Description of Study Area

3.1.1. Location and area

Gondar, the capital town of north Gondar administrative zone is located in the north-west of the capital city of the Federal Democratic Republic of Ethiopia, Addis Ababa at a distance of 727 Km along Debre Markos road and 162 Km to the capital of Amhara National Regional State, Bahir Dar. Geographically it is located between 12°26′20″ to 12°41′10″ N Latitudes and 37°21′35″ to 37°32′31″ E longitudes. The total area coverage of the study area is 292.37 km^2 (Figure 3.1).

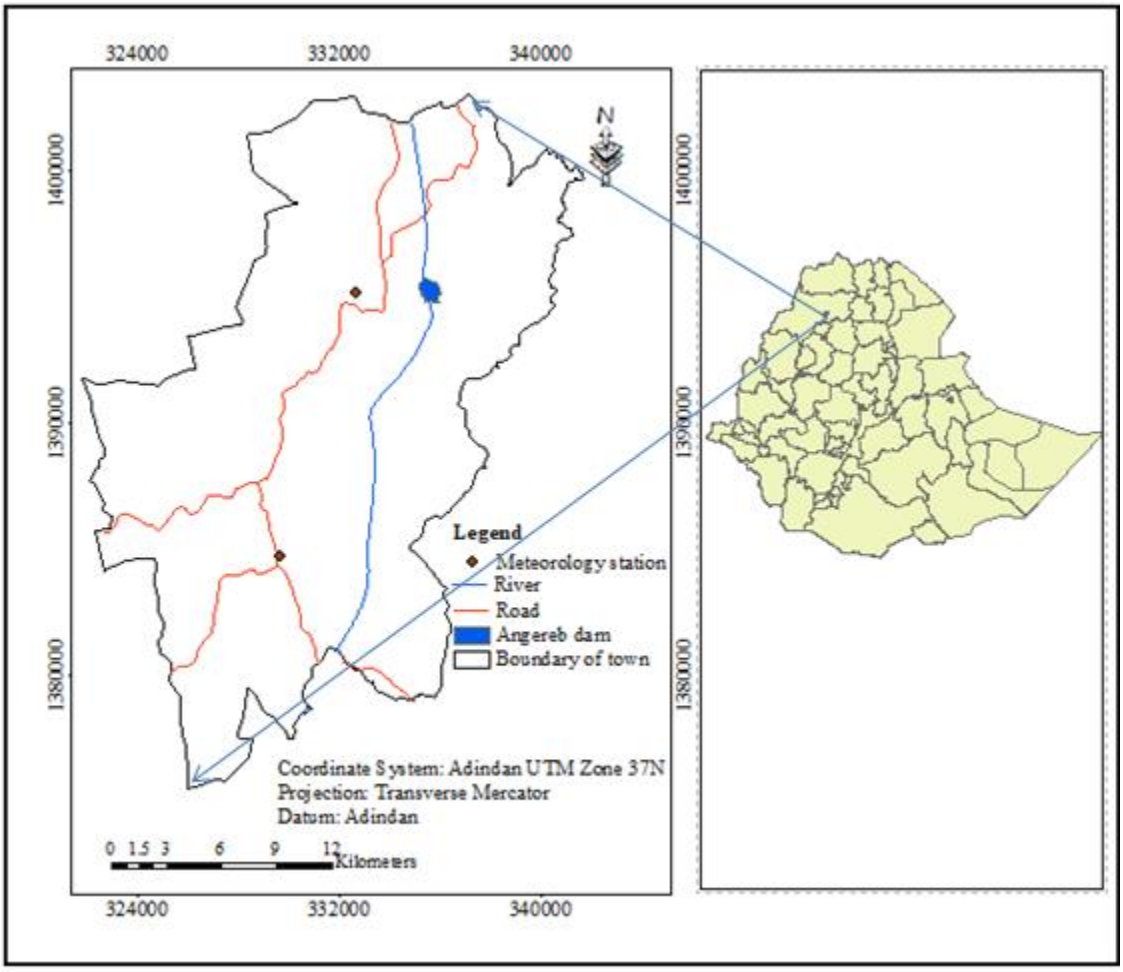

Figure 3.1: Location map of the town.

3.1.2. The topography of the study area

Topography describes the shape and feature of the earth's surface and other related phenomena or it is an integral part of the land surface. Landforms, elevation, latitude, longitude, and topographic maps are included in topography. The topography of Gondar town is rugged. The elevation of the town varies from 1835m in south and southeast to 2771m in north and northwest of the town.

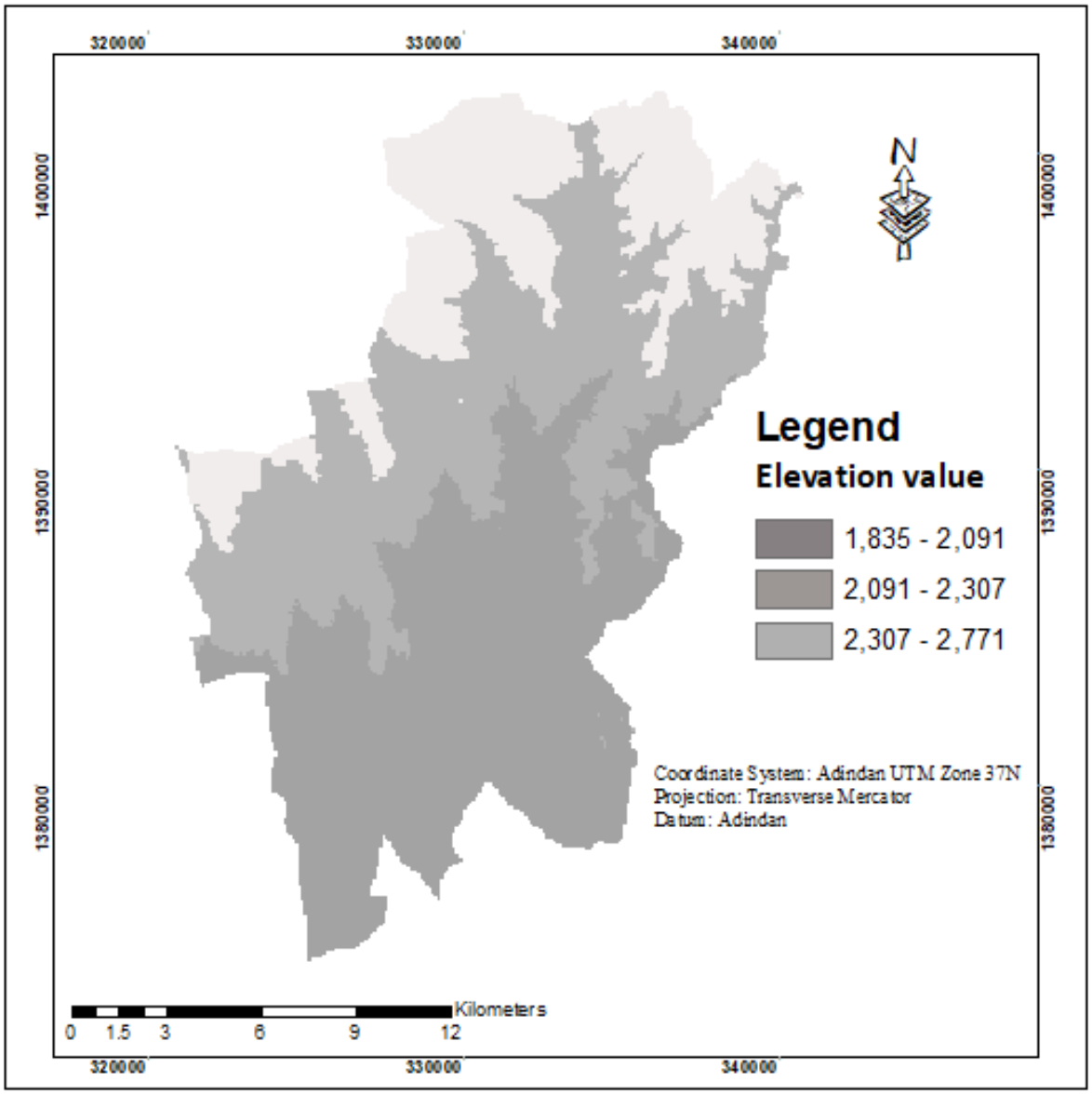

Figure 3.2: The elevation map of the town (m)

3.1.3. Population

According to CSA (1994), the population of the Gondar town was 112,249 in 21,695 households, of whom 51,366 (45.76%) were males and 60,853(54.24%) were females. Amhara, the Tigrayan, and Qemant ethnic groups were living in Gondar town which accounts for 88.91%, 6.74%, and 2.37% correspondingly; all other ethnic accounts for 1.98% of the population. 97.57% of the population of Gondar town spoke Amharic as the first language, and 1.67% spoken Tigrinya; the remaining 0.76% spoke all other primary languages. Gondar was once the home of a large

population of Ethiopian Jews, most of them immigrated to Israel in the late 20th and early 21st century. The population increases to 207,044 in 2007, of whom 98,120 (47.39%) were men and 108,924 (52.61%) were females (CSA, 2007). In addition to this, the population projection figure of the town had shown that 155,860 (48.12%) were male and 168,040 (51.88%) were female inhabitants from the total population of 323, 900, (CSA, 2015). The detailed population distribution of Gondar town is presented in figure 3.2.

	Male	Female	Total
1994	51366	60853	112249
2007	98120	108924	207044
2015	155860	168040	323900

Source: CSA data

Figure 3.3: The population distribution of the town.

3.2. Climate

3.2.1. Temperature

Based on temperature recorded at Gondar meteorology station through the study period (from 1988 - 2018), the maximum mean monthly temperature was very high from February - May. However, from these months, the maximum mean monthly temperature was very high during April which was 30.22 ℃. Whereas, the lowest maximum mean monthly temperature recorded from June - September, mainly in July which was 23.14℃. Additionally, the highest minimum

mean monthly temperature of the town was 15.95℃, which was occurred in April and the lowest was in December (which is about 12.04 ℃). Therefore, April and December are the warmest and the coldest months correspondingly in and around Gondar town (figure 3.4).

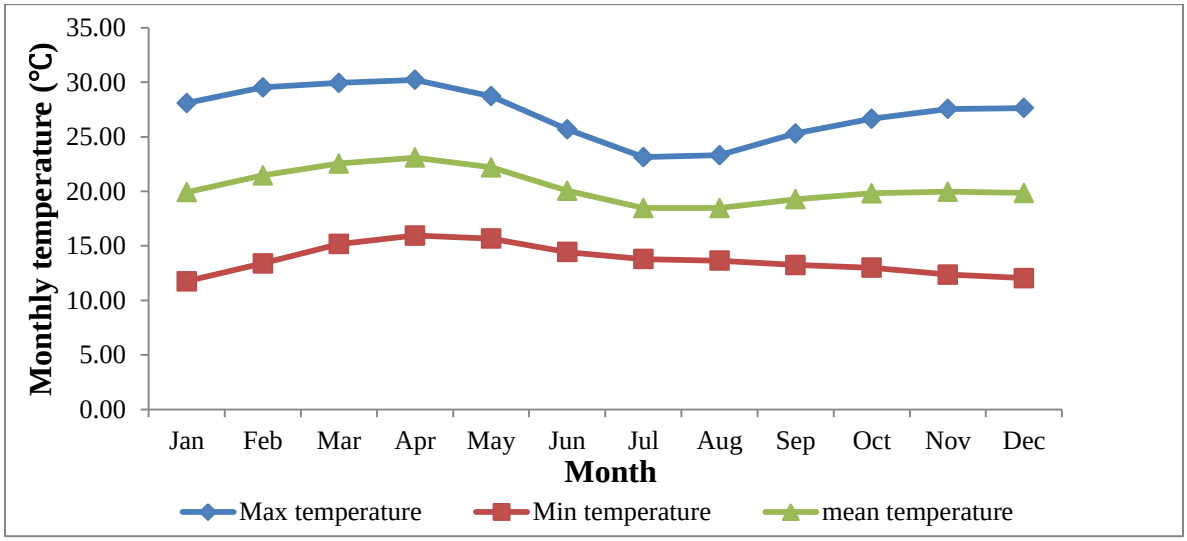

Source: NMA data

Figure 3.4: Maximum, minimum, and mean monthly temperature distribution from 1988-2018.

Even if there were variations in temperature from month to month in a year due to the variations in climate parameters, on average the temperature was increased from the year 1988 to 2018, particularly, the temperature has been relatively increasing after 2011 (Figure 3.2).

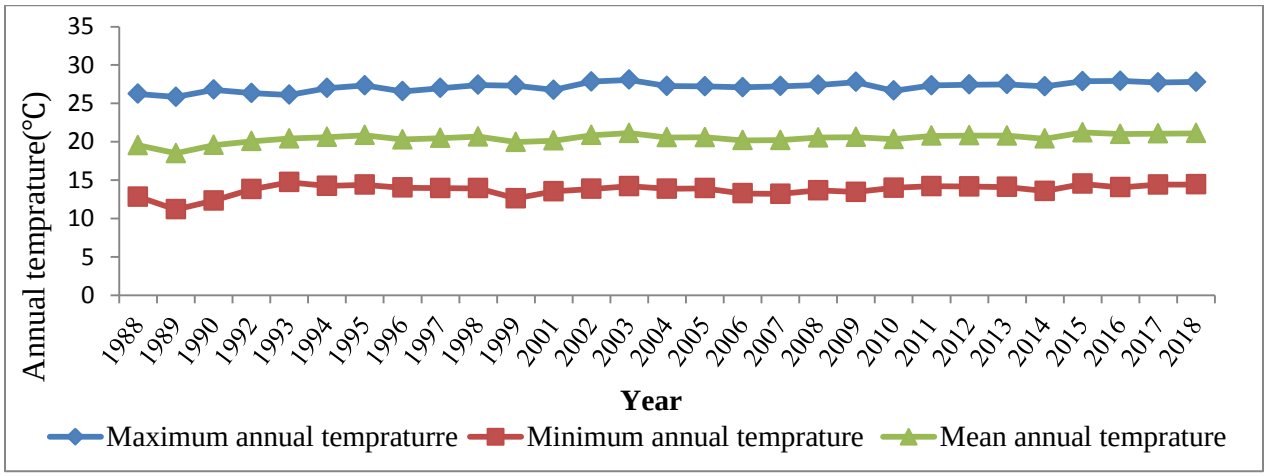

Source: NMA data

Figure 3.5: Maximum, minimum, and mean annual temperature distribution from 1988-2018.

3.2.2. Rainfall

The data recorded at Gondar meteorological station from 1988 - 2018 shows monthly average rainfall of the town was 1172.25mm and the maximum and minimum monthly average rainfall was 318.98 mm and 1.84 mm, which is recorded in July and January. On average, rainfall was very high in June, July, August, and September since these are rainy months in most parts of Ethiopia. Whereas October and May have moderate rainy months and January, February, March, April, November, and December are the dry months (Figure 3.6).

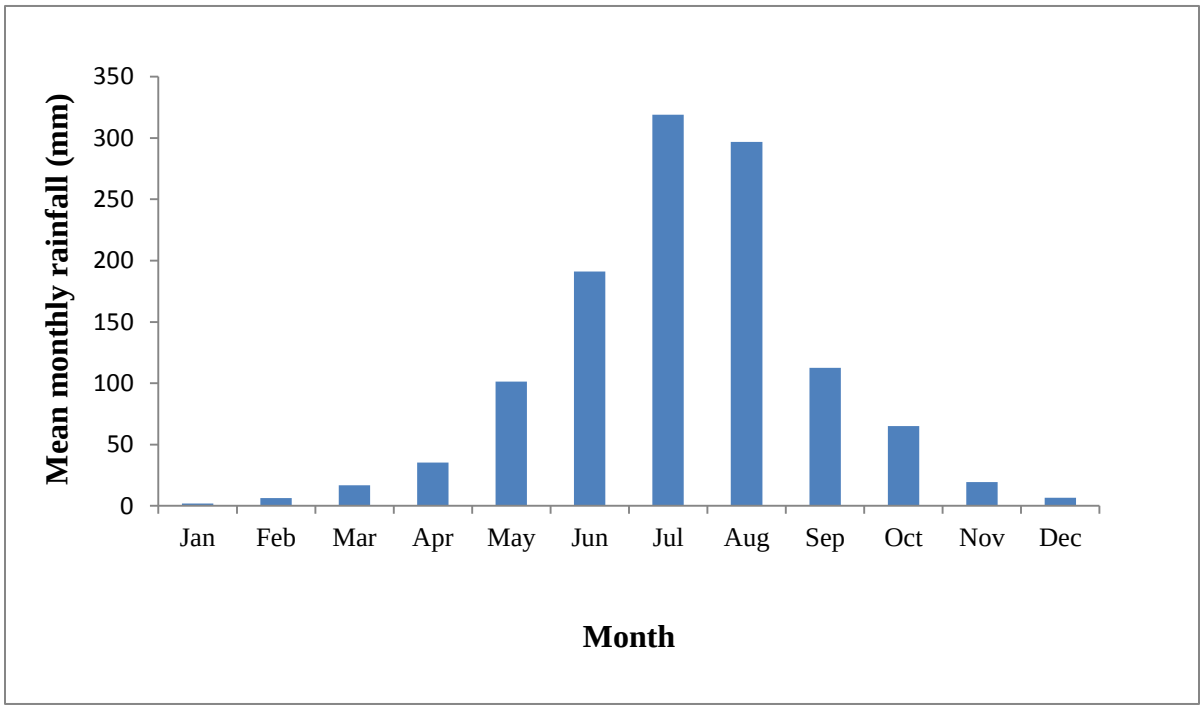

Source: NMA data

Figure 3.6: Mean monthly rainfall distribution from 1988-2018

Based on the figure provided below, the mean annual rainfall of Gondar town from 1988 to 2018 ranges from 83.45 mm to 152.90 mm. The mean annual rainfall was varying from year to year within 31 years of the study period, mostly due to the variations of climate and weather parameters (Figure 3.7).

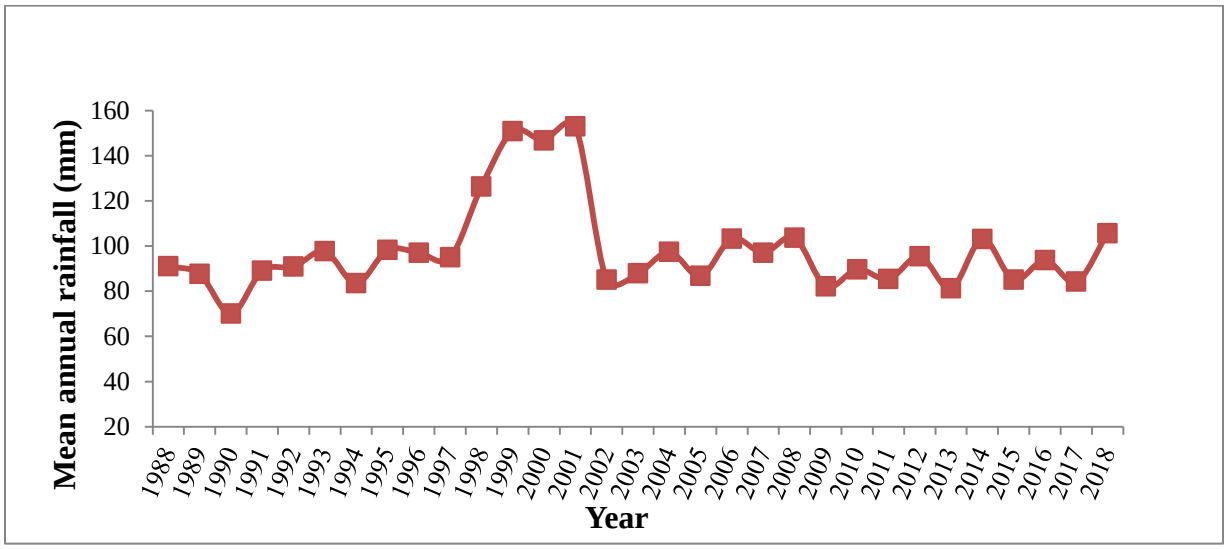

Source: NMA data

Figure 3.7: Mean annual rainfall distribution from 1988 - 2018

The maximum annual rainfall recorded in Gondar town was 1834.77 mm which was recorded in 2014 and the minimum annual rainfall recorded in the town was 840.82 mm in 1990 from 1988 - 2018. The distribution of annual rainfall of Gondar town from 1987 to 2018 is provided in Figure 3.8.

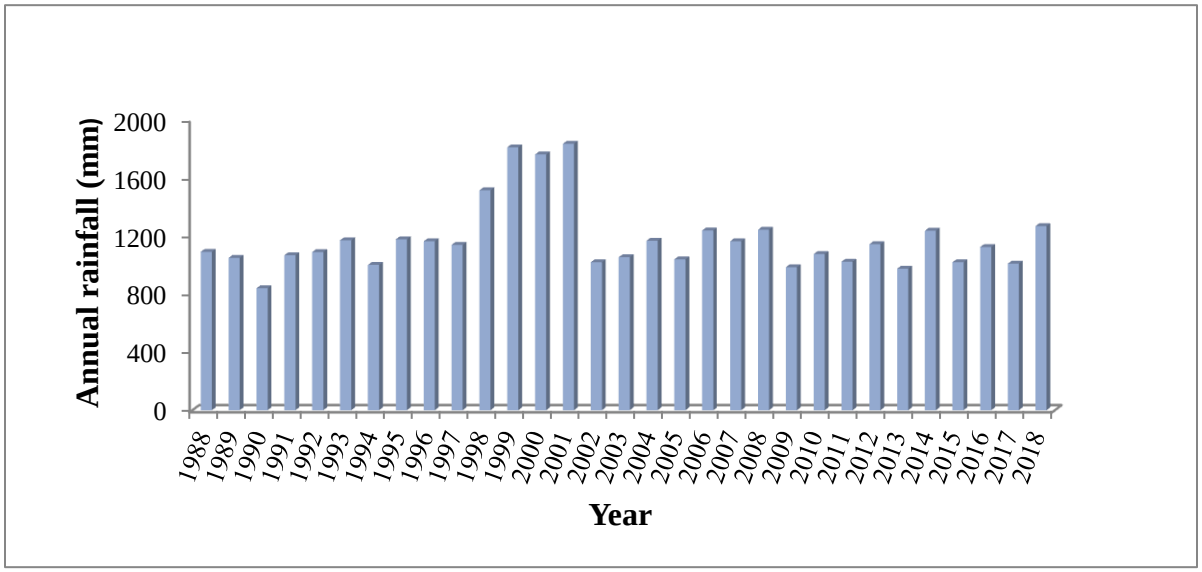

Source: NMA data

Figure 3.8: Annual rainfall distribution from 1988-2018.

3.3. Datasets and Sources

3.3.1. Remotely Sensed Data

The Landsat image acquired by Landsat 5 TM, Landsat 8 OLI/TIRS, and MODIS were used to conduct this research. Landsat 5 and 8 were downloaded from the USGS website (http://earthexplorer.usgs.gov) accessed in June 2019, whereas MODIS was downloaded from (https://earthdata.nasa.gov/about/daacs/daac-lpdaac) website accessed in August 2019 respectively, which is free of charge by using path 169 and row 053 of land sat satellite series. Due to the problem of poor resolution of MSS sensor and data availability, the study period covered only from the year 1988 to 2018. Thus, the years 1988, 2002, and 2018 were selected for analysis with 14 and 16 years intervals. Imageries that were acquired during December were used, because, cloud and haze-free imageries can easily be obtained during dry seasons where there is no cloud cover and rain and avoid the effects of annual crops. The detailed description of Landsat data, which was used to access LULC change, NDVI, and LST distribution of the town provided below in table 3.1.

Table 3.1: Remote sensing datasets were used for the study and its descriptions.

path/row	Acquisition date	Satellite	Sensor	Resolution PAN/MS/TIRS	Source
169-053	12/26/1988	Landsat	TM	15/30/120	USGS
	12/15/2002		TM	15/30/120	
	12/13/2018		OLI	15/30/100	
	12/13/2018	Terra	MODIS	1KM	LP DAAC

A) Landsat Thematic Mapper (TM)

Landsat Thematic Mapper (TM) sensor was carried on Landsat 4 and Landsat 5 starts from July 1982 -May 2012. It has seven spectral bands; from these bands, three in the visible, three in infrared, and one in the thermal region of the spectrum. TM image has a spatial resolution of 30m for MS (band 1 to 5 and 7) and 120 m for thermal (band 6). Therefore, TM Band 6 is specifically sensitive to thermal infrared radiation to measure the LST of the earth's surface. Additionally, TM has a temporal resolution or repeat the cycle of 16 days. The scene size of TM

images is approximately 170 km north-south and 183 km east-west. Detail about thematic mapper sensor bands and other descriptions are provided in Table 3.2.

Table 3.2: Landsat 5 TM sensor description

Landsat 5	Bands	Description	Wavelength (μm)	Temporal resolution (day)	Spatial resolution (m)
Thematic mapper	1	Blue	0.45 - 0.52	16	30
	2	Green	0.52 - 0.60	16	30
	3	Red	0.63 - 0.69	16	30
	4	NIR	0.76 - 0.90	16	30
	5	SWIR-1	1.55 - 1.75	16	30
	6	Thermal	10.40 - 12.50	16	120
	7	SWIR-2	2.08 - 2.35	16	30

NB: NIR-near infrared, SWIR-short wave infrared

B) Landsat Operational Land Imager (OLI) and Thermal Infrared Sensor (TIRS)

Landsat 8 was launched on February 11, 2013, with OLI and TIRS. It has 11 bands; from these bands, 1 to 7 and 9 is MS, and band 8 is panchromatic while band 10 and 11 are thermal, which is used to determine LST. The spatial resolution of Landsat 8 is 15 m, 30 m, and 100 m for PAN, MS, and TIRS respectively. Band 1 is ultra-blue useful for coastal and aerosols studies while Band 9 is useful for cirrus cloud detection. The scene size of Landsat 8 images is 170 km north-south and 183 km east-west (USGS, 2013). Detail explanation about OLI and TIRS bands are provided in Table 3.3.

Table 3.3: Landsat 8 OLI and TIRS bands description

Landsat 8	Bands	Description	Wavelength(μm)	Temporal resolution (day)	spatial resolution (m)
OLI and TIRS	1	Ultra-blue	0.43 - 0.45	16	30
	2	Blue	0.45 - 0.51	16	30
	3	Green	0.53 - 0.59	16	30
	4	Red	0.64 - 0.67	16	30
	5	NIR	0.85 - 0.88	16	30
	6	SWIR-1	1.57 - 1.65	16	30
	7	SWIR-2	2.11 - 2.29	16	30
	8	Panchromatic	0.50 - 0.68	16	15
	9	Cirrus	1.36 - 1.38	16	30
	10	TIRS-1	10.60 - 11.19	16	100
	11	TIRS-2	11.50 - 12.11	16	100

NB: NIR-Near infrared, SWIR-Short wave infrared, and TIRS-thermal infrared sensor.

3.3.2. Meteorology Data

Meteorological data such as humidity, temperature, and rainfall data were gathered from the National Meteorological Agency of Ethiopia. These data were used to define the climate of the Gondar town through the study periods and humidity that comes from meteorology was used to calculate water vapor content in the atmosphere, during LST determination in Landsat 8 with SWA.

3.3.3. Ground Truth Data and Google Earth Data

Ground truth data were collected from the field using GPS after stratified sample points generated from the image of Landsat and their coordinates from Google Earth. Field data were used for validating the LULC classified image into different classes by observing the real LULC of the town. To minimize errors in classification, pictures showing different LULC classes in the town were captured. Google Earth map was used as a visual interpretation during the image classification process. According to Jensen (2015), Lillesand et al. (2008), and Congalton and Green (2009) a minimum of 50 sample points for each mapping class should be collected for maps of < 4,000 km2 in size and fewer than 12 classes to do accuracy assessment. The area in and around Gondar town is 29237.1 ha (292.371km2) and five LULC classes were identified for

this study. Therefore, the eighty-five sample points were collected for this study to accuracy assessment and classification. From this 50% of the sample, points were used for accuracy assessment and the remaining 35% of sample points were used for training site during image classification.

3.3.4. MODIS Data

Moderate Resolution Imaging Spectroradiometer data were used to validate the LST extracted from Landsat imageries. This MODIS data were downloaded from the National Aeronautics and Space Administration Land Processes Distributed Active Archive Center (NASA LP DAAC) website (https://earthdata.nasa.gov/about/daacs/daac-lpdaac) accessed in August 2019.

3.4. Software

ERDAS IMAGINE 2014, ArcGIS 10.5, Google Earth PRO 2017, Microsoft word and excel 2010, XLSTAT 2014 and 2019, and easy GPS was used to process satellite imageries and analyze urban LULC changes, NDVI, NDBI, LST, and the association LST with LULC indices. From this, ERDASIMAGINE 2014 was used for image preprocessing and image classification. Arc GIS10.5 was used to prepare the layout map of the town, zonal statistics, and reclassification. Mapping of NDVI, NDBI, and LULC map of a town, conversion detection analysis and extract LST were also done by ArcGIS 10.5. While, Google Earth PRO 2017 was used as a base map in visual image interpretation, and generate coordinate points for the image of 2018. XLSTAT 2014 and 2019 were used to develop correlation statistics of LST with NDVI and NDBI. Easy GPS was used to download point data from handheld GPS for accuracy assessment and Microsoft word and excel 2010 also used to compile the whole parts of this study.

3.5. Methods of analysis

This project has four main methods. The first was the urban LULC analysis from Landsat 5 and 8. The second one is the calculation of LST, NDVI, and NDBI from Landsat imageries. Estimation of LST from the MODIS data set in the third step. Finally, zonal and correlation statistics were done for NDVI and NDBI with LST. The general methodology for data processing is described in the following flow chart.

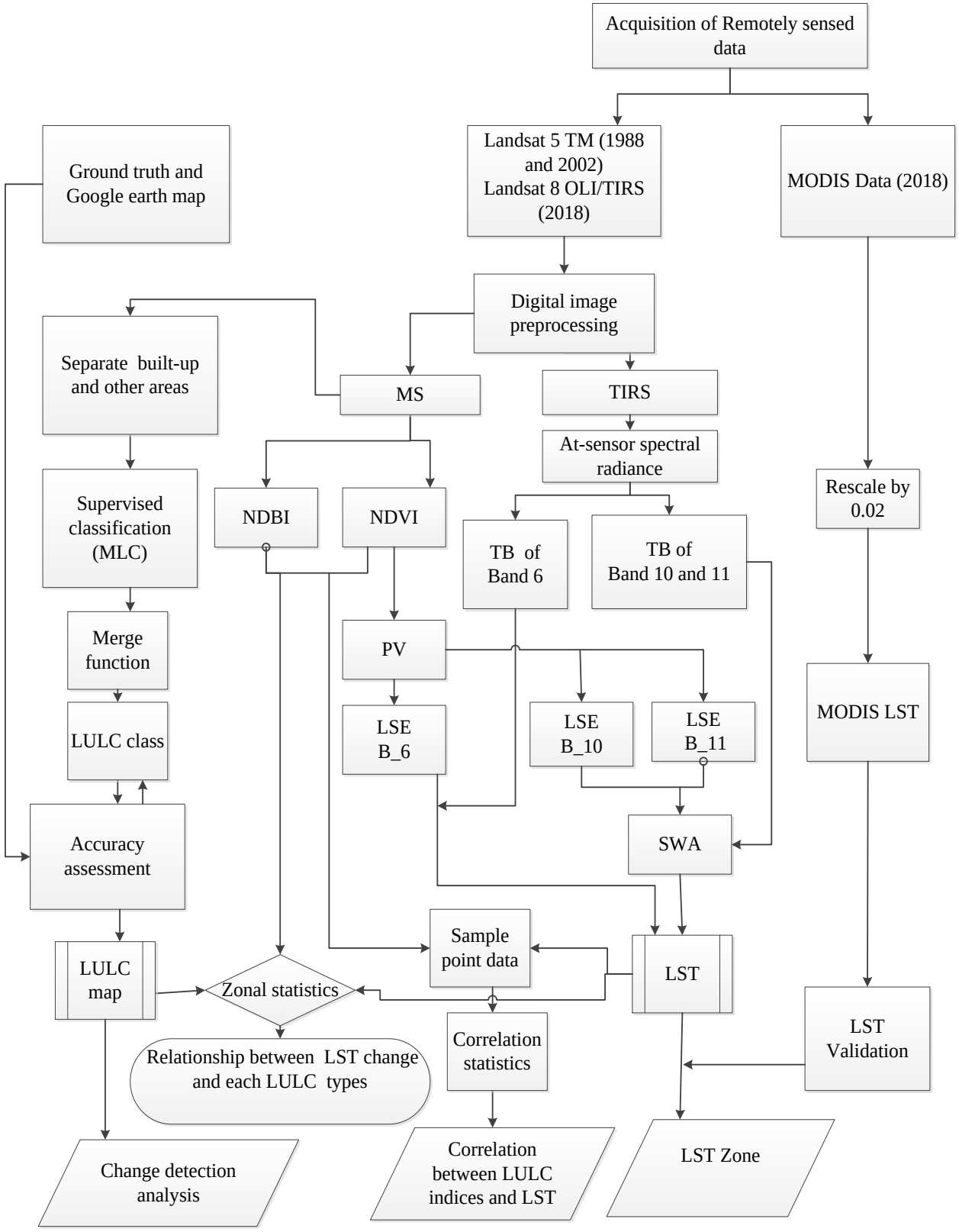

Figure 3.9: Flow chart of methodology.

3.5.1. Digital Image Preprocessing

Satellite imagery is affected by various factors, which decrease the image quality. Therefore, to get important information from those images, they should be processed and corrected digitally before using them for further analysis. Digital image processing involves the operation and interpretation of digital images through the help of computer application software. It is helpful to increase the quality of an image and maintain the quality image for interpretation and classification; it is possible to minimize interpretation errors since the image can easily be manageable on a computer (Abel, 2018). Therefore, preprocessing mostly comprises a series of sequential processes, including atmospheric correction or normalization, image registration, and geometric correction. Digital image pre-processing functions include those processes that are essential before using information extraction for data analysis.

3.5.2. Multispectral Radiometric Correction

Preprocessing is very essential to get an accurate image because radiation, which comes from the source, always interacts with the atmosphere (Abel, 2018). The energy, which is reflected to the sensor after its contact with the target objects is useful for remote sensing. Therefore DN should be converted into spectral radiance. Landsat 5 TM image was radiometrically corrected and spectral radiance converted to radiance in Arc GIS by using the following formula (Markham and Barker, 1986):

$$L\lambda = \frac{L\lambda max - L\lambda min}{Qcalmax - Qcalmin} * (Qcal - QCALmin) + L\lambda min \quad \text{..... (1)}$$

Where; Lλ is Spectral radiance received by the sensor (W/ (m2 * sr * μm)),QCAL is the quantized calibrated pixel value in DN of band 6, Lλmin is the spectral radiance that is scaled to Qcalmin (W/ (m2 * sr * μm), Lλmax is the spectral radiance that is scaled to Qcalmax (W/ (m2 * sr * μm), Qcalmin is the minimum quantized calibrated pixel value (corresponding to Lλmin in DN which is 1) and Qcalmax is the maximum quantized calibrated pixel value (corresponding to Lλmax in DN which is 255). Then, level pixel DN values were converted to top of atmospheric (TOA) reflectance using the equation provided below:

$$P\lambda = (\pi * L\lambda * d\hat{}2) / (ESUN\lambda * \cos\theta) \quad \text{..... (2)}$$

Where; Pλ is unit less planetary reflectance, Lλ is Spectral radiance at the sensor's aperture, d is Earth-Sun distance in astronomical, ESUNλ is mean solar exo-atmospheric irradiances and θ is solar zenith angle in degrees.

Landsat 8 OLI image is also radiometrically corrected and spectral radiance changed to radiance in ArcGIS using the formula given by (USGS, 2016):

$L_\lambda = M_\lambda * Q\text{cal} + AL$……..…… (3)

Where; L_λ = Spectral radiance (W/ (m2* sr * μm)); $M\lambda$ is Radiance multiplicative scaling factor for the band (radiance_mult_band_n from the metadata); AL is Radiance additive scaling factor for the band (radiance_add_band_n from the metadata); Qcal is Level one pixel value in DN. Then, level 1 pixel DN values were converted to top of atmosphere reflectance using the equation (USGS, 2016):

$\rho\lambda' = Mr * Q\text{cal} + Ar$…….. (4)

Where; ρλ′ is Top-of-Atmosphere Planetary Spectral Reflectance, before correction for a solar angle, Mr is Reflectance multiplicative scaling factor for the band (reflectance_mult_band_N from the metadata), Ar is the Reflectance additive scaling factor for the band (reflectance_add_band_N from the metadata), and Qcal is Level one pixel value in DN. Once a solar elevation angle is selected, then conversion to true top of atmosphere reflectance is given by:

$P\lambda = \rho\lambda' / \cos \theta_{SZ}$…….. (5)

Where: ρλ′ = Top-of-Atmosphere Planetary Reflectance; θSZ = Local solar zenith angle.

3.5.3. Image Classification

According to Gao (2009) and Lillesand *et al*. (2004), image classification is a technique of extracting information from the image based on the reflectance value of an object. The class can be grouped into a thematic layer of having similar urban LULC in the image. It is the most common method to extract information in digital remote sensing. A human analyst uses the components of visual interpretation to recognize homogenous groups of pixels, which represent different land cover classes of interests to classify features of an image. The spectral information

is characterized by the DN in each spectral band and assumes to classify each pixel based on spectral information.

Image classifications using remote sensing procedures have attracted the devotion of the research community because classification is the backbone of environmental, social, and economic applications (Lu and Weng, 2007). Multispectral data were used to classify the spectral pattern presented in each pixel used as the numerical basis for categorization. This concept is called Pattern Recognition. The definition of spectral pattern recognition is the family of classification procedures that utilizes this pixel-by-pixel spectral information as the basis for automated land covers classification (Ziena, 2017). To do this supervised classification with maximum Likelihood Classifier technique was used.

3.5.3.1. Supervised Classification

The supervised classification technique uses a training sample for each category, that is, a group of data points known and come from the class of interest. The classification was done by considering how close a point to be categorized is to each training sample. The Supervised classification has different techniques such as maximum likelihood, parallelepiped, and minimum distance to mean. This study uses supervised classification because it has an advantage in regards to the development of information classes, self-assessment by using training sites and training sites reusable. However, information classes may not match spectral classes, the signature homogeneity, and uniformity of information classes may vary.

3.5.3.1.1 The Maximum Likelihood Classifier Technique

The maximum Likelihood of supervised classification is used statistics (mean, variance, or covariance) to classify pixel values. The MLC technique applies the probability theory to the classification task. This method defines the class centers and the variability in raster values in each input band for each class from the training set classes. The information allows the procedure to define the probability that an assumed cell in the input image belongs to a specific training set class center and the size and shape of the class in spectral space. It calculates all of the class probabilities for every raster cell and gives the cell to the class with the highest probability value. This technique yields more accurate class assignments than the minimum distance to means

technique when classes vary significantly in size and shape in spectral space (Lillesand *et al*., 2004).

The MLC quantitatively defines both the variance and covariance of a class spectral response patterns when classifying unidentified cells. We may compute the statistical probability of an assumed cell value being a member of a particular land class, the computer would calculate the probability of the cell value occurring in the distribution of class then the likelihood of its occurring in class. After assessing the probability in each category, the cell would be allocated to the highest probability value class. The MLC technique has its weakness and strength. The weakness of this procedure is computational ineffective compared to the other technique. The strength of this technique is advantageous for different degrees of variance in the spectral response data. Therefore, to do this study, the MLC technique was used. Because in urban areas, there are different degrees of variance in spectral response data. There is a problem of cell mixing especially in low-resolution imageries such as Landsat and this has seriously affected the urban LULC classification accuracy of the study. To minimize this problem in image classification, a Google Earth map, field survey data, and an aerial photo were used.

Generally, the image classification process was conducted based on the following procedures in this study.

- Initially, separate the total study area into data groups namely the built-up area and the remaining areas. These are used to avoid the challenges of pixel mixing of the built-up areas and agricultural land.
- Classified the two data groups separately.
- The classified images (raster) were converted to polygon (vector).
- Merge these two polygon images to form one single image for the study area.
- Then, the merged image of the Gondar town was converted to raster.
- Finally, the correctness of a classified image was done.

After classification accuracy was conducted, final LULC thematic layers were identified and mapped for three study periods (1988, 2002, and 2018). Therefore, Gondar town has the following LULC classification schemes such as built up, vegetation, agriculture, water body, and bare land. This classification scheme was developed based on (Anderson *et al.*, 1976) the first level of the classification scheme, and has been made to provide as much compatibility as

possible with other classification systems. Currently, this is being used by the various Federal agencies involved in land use inventory and mapping such as the Ethiopian Mapping Agency, based on prior knowledge and a brief reconnaissance survey in the study area.

3.5.4. Accuracy Assessment

The accuracy of the classification was checked to extract reliable information after image classification. As Gao (2009) states accuracy assessment is a comparison of image interpretation by a computer with the aid of ground truth data. For this comparison, fifty sample points that are collected on the ground using handheld GPS and Google earth maps were used to check the correctness of classification (Amare, 2015). These sample points per each LULC class were collected to develop the confusion/error matrix and it is used for accuracy assessment. It was calculated to assess the association of reference pixels with classified land use and land cover maps. The arrangement of at error/confusion matrix was numbered representing the number of samples allocated to each class comparative to the reference data, in records and fields. The records indicate LULC maps derived from classification while fields indicate reference data collected from the field. The advantage of error/confusion matrix is to determine different statistical values like producer's accuracy (omission error), user's accuracy (commission error), overall accuracy, and kappa coefficient used to assess accuracy assessment (Congalton and Green, 2009).

Producer's accuracy is calculated by dividing the diagonal elements in each category by the sum of pixels of that category which is calculated from the reference data. This statistic shows the chance of a reference data being exactly classified and is a measure of omission error or error of exclusion. The producer's accuracy can be calculated based on the following equation.

$$\text{producer's accuracy} = \frac{\text{number of corrected pixels in a class}}{\text{total sample points in a class}} * 100 \quad \ldots\ldots\ldots\ldots\ldots\ldots\ldots\ldots\ldots 6$$

User's Accuracy is calculated by dividing the diagonal elements in a category by the sum of pixels that were classified in that category, the result is a measure of commission error or error of inclusion. It is calculated based equation provided below.

$$\text{User's accuracy} = \frac{\text{number of corrected pixels in a class}}{\text{total number of classified points in a class}} * 100 \quad \ldots\ldots\ldots\ldots\ldots\ldots\ldots\ldots\ldots 7$$

Overall accuracy is calculated by the sum of exactly classified pixels divided by the sum of sample points (Congalton, 1991). It includes only the diagonal elements of the error matrix and it is hard to relate unalike overall accuracy values if an unalike number of accuracy sites were used. The value of overall accuracy was calculated based on the following equation provided below.

$$\text{Overall accuracy} = \frac{\text{the sum of correctly classified pixels}}{\text{total sample points}} * 100 \ldots\ldots\ldots\ldots\ldots\ldots\ldots\ldots\ldots\ldots (8)$$

Kappa analysis is used to show the variation between actual agreements and the agreement anticipated by chance. It includes both diagonal and non-diagonal elements of the error matrix (Tempfli *et al*., 2009). Kappa analysis gives Khat statistics which is the measure of an agreement (Congalton, 1991). This study uses khat statistics because it considers non-diagonal elements and compares two classification products statically. It is calculated by the following equation provided below:

$$k = \frac{\mathrm{N}\sum_{\mathrm{i}=1}^{\mathrm{r}} \mathrm{Xii} - \sum_{\mathrm{i}=1}^{\mathrm{r}} (\mathrm{Xi+} * \mathrm{X+i})}{\mathrm{N}^2 - \sum_{\mathrm{i}=1}^{\mathrm{r}} (\mathrm{Xi+} * \mathrm{X+i})} \ldots\ldots\ldots\ldots\ldots\ldots\ldots\ldots\ldots\ldots\ldots\ldots\ldots\ldots\ldots\ldots\ldots\ldots\ldots\ldots\ldots\ldots (9)$$

Where: N- total number of samples included in the matrix, Xii- number of observations in row i and column i, Xi+-total observations in row i, and X+i- total observations in column i. The value of K falls between 0 and 1, where the former and later indicates no better than would be expected by chance and perfect agreement respectively. This value is often multiplied by 100 to give a percentage measure of classification accuracy (Worku, 2018).

3.5.5. Urban Land use and Land cover Thematic Layer of the town

Five LULC thematic layers were determined and mapped for 1988, 2002, and 2018 after classification accuracy was done. Therefore, Gondar town has the following LULC classes and is presented in table 3.5.

Table 3.4: Urban LULC thematic layer of the town.

NO.	LULC classes	Descriptions
1	Built-up	The area is occupied by buildings including mixed and pure residences, factories, offices, churches, schools, mosques, hospitals, hotels, roads, and warehouses.
2	Agriculture	The area covered by annual and perennial crops
3	Vegetation	The area covered by shrubs, tree, and grassland
4	Bare land	The area covered by day soil, sand/rock and, dry salt flats, beaches, a non-vegetated area dominated by rock, eroded and degraded lands
5	Waterbody	The area covered by river and dams

3.5.6. Change Detection Analysis

Change detection was carried out by using the post-classification method. Post classification is the most commonly used approach for change detection purposes (Xiuwan, 2002). The analysis of LULC Change maps involved technical procedures of integration using ArcGIS software techniques. The first task is to develop a table indicating the area coverage in hectare and the percentage change for each year 1988, 2002, and 2018 measured against each LULC class. Therefore, to calculate the rate of LULC Change, the following percentage equation was used (Lambin *et al*., 2001).

$$\text{Percentage area change} = \frac{\text{area i year x+1} - \text{Area i year x}}{\sum_{\text{i=1}}^{\text{r}}(\text{Area i year x+1})} \text{ x } 100 \quad \text{..... (10)}$$

Where; Area i year x = area of cover i at the previous year, Area i year x +1 = area of cover i at the next year, $\sum_{i=1}^{r}(Area\ i\ year\ x+1)$ is the total cover area in the next year.

3.5.7. Determination of the land use land cover indices

3.5.7.1. Normalized Difference Vegetation Index

This is very essential to discriminate vegetation from no-vegetation and indicates the amount of vegetation present on the surface. In addition to this, NDVI computation is important to calculate the emissivity (ε). Since, these parameters are highly associated with the NDVI (Weng *et al*., 2004). Therefore, NDVI was acquired from the red bands in spectral reflectance measurements

and near-infrared bands in the ArcGIS software. The NDVI was calculated by the following equation.

$$\text{NDVI} = \frac{\text{Near-infrared} - \text{Red}}{\text{Near-infrared} + \text{Red}} \ldots \ldots \ldots \ldots \ldots \ldots \ldots \ldots \ldots . \ldots \ldots \ldots \ldots \ldots \ldots \ldots \ldots \ldots \ldots \ldots \ldots \ldots \ldots (11)$$

Where; NDVI is Normalized Difference Vegetation Index

3.5.7.2. Normalized Difference Built-up Index

This index is very important for mapping urban or built-up areas from Landsat data. It is useful to recognize the extent and density of imperviousness surfaces like built-up, asphalt road, and parking areas and map these areas (Zha *et al*., 2003 and Malik *et al.*, 2019). Urban areas have a higher reflectance value in the SWIR region than the NIR region (Alhawiti and Mitsova, 2016). The NDBI can be calculated using short wave and near-infrared bands of the Landsat image in the following way.

$$\text{NDBI} = \frac{\text{Short wave infrared} - \text{Near infrared}}{\text{Short wave infrared} + \text{Near infrared}} \ldots \ldots \ldots \ldots \ldots \ldots \ldots \ldots \ldots \ldots \ldots \ldots \ldots \ldots \ldots \ldots \ldots \ldots \ldots \ldots (12)$$

Where; NBDI-Normalized difference built-up index

3.5.8. Land Surface Temperature Computation

The land surface temperature can be calculated in different ways based on the parameters (for instance, normalized difference vegetation index, emissivity, water vapor, and resources (data and software) was used.

3.5.8.1. Land Surface Emissivity

According to Becker and Li (1995), Emissivity is the ratio of the radiance which is emitted by the real surface materials at their temperature and the radiance emitted by the black body at the same temperature. Emissivity can be represented by the function of wavelength is controlled by several environmental factors such as surface water content, chemical composition, structure, and roughness. For vegetated areas, emissivity varies significantly with types of plants, areal densities, and growth rates. Land surface emissivity is closely associated with NDVI (Weng and Larson, 2005, Tran and Ha, 2010). Therefore, the emissivity value can be calculated by the following equation provided below in different NDVI values (Sobrino *et al.*, 2001).

$$E = \begin{cases} Ew & NDVI < 0 \\ Es & 0 \geq NDVI < 0.2 \\ EvPv + Es(1 - PV) + Ce & 0.2 \geq NDVI < 0.5 \\ Ev & NDVI \geq 0.5 \end{cases} \quad .. \quad (13)$$

Where; *Ev*- emissivity of vegetation; *Es*- emissivity of soil; *Ce*-is the surface geometrical distribution is given by (1-Es) + (1-Ev)*F*Ev, and F=0.55, shape parameters factor considering different geometrical distribution and Pv-proportion of vegetation which is calculated based on the equation provided below (Jin et al., 2015).

$$PV = \left(\frac{NDVI - NDVI_{min}}{NDVI_{max} - NDVI_{min}}\right)^2 \ldots\ldots (14)$$

Where; PV is Proportion of Vegetation, NDVI is Normalized Difference Vegetation Index, NDVI min is the Normalized Difference Vegetation Index minimum value and NDVImax is the Normalized Difference Vegetation Index maximum value.

The emissivity value of soil, water, and vegetation of Landsat 5 and 8 thermal bands are presented in table 3.6.

Table 3.5: land surface emissivity value of Landsat 5 and 8 thermal bands.

Satellite	thermal bands	water	soil	Vegetation
Landsat5	6	0.995	0.974	0.986
Landsat8	10	0.996	0.973	0.984
Landsat8	11	0.984	0.97	0.98

3.5.8.2. Land Surface Temperature Algorithms

After spectral radiance is converted to radiance, the raw digital numbers of the thermal bands are converted to Top of Atmosphere brightness temperatures, which are the effective temperature viewed by the satellite under an assumption of emissivity (Chander *et al*., 2009) using Planck's equation provided below:

$$TB = \frac{K2}{\ln(\frac{K1}{L\lambda} + 1)} \ldots\ldots (15)$$

Where; *T*B is effective at-sensor brightness temperature (K), *K*2 is calibration constant 2 (K), *K*1 is calibration constant 1 (W/ (m2 * sr * μm)), $L\lambda$ is spectral radiance at the sensor's aperture (W/ (m^2 * sr * μm)) and ln is natural logarithm.

Table: 3.6: calibration constants for thermal bands in different Landsat series

satellite	band number	K1	K2	$L_\lambda$min	$L_\lambda$max	M_λ	AL
Landsat 5	6	607.76	1260.56	1.2378	15.303	_	_
Landsat 8	10	774.8853	1321.0789	_	_	0.0003342	0.1
Landsat 8	11	480.8883	1201.1442	_	_	0.0003342	0.1

For Landsat 5, the LST can be determined by this equation (Xiong *et al*., 2012, Yue *et al*., 2007).

$$\mathrm{LST} = \frac{\mathrm{TB}}{1+\left(\lambda*\frac{\mathrm{TB}}{\mathrm{p}}\right)*\ln\varepsilon} \ldots\ldots (16)$$

Where; LST is land surface temperature in kelvin, TB is sensor brightness temperature in kelvin, λ (11.45) is the wavelength of the emitted radiance (for peak response and average limiting wavelengths), ε is land surface emissivity. $p = \frac{hc}{\sigma}$=1.4388*10^{-2} MK, where, h is Plank's constant (6.626*10^{-34}Js, C indicates light velocity (2.998*10^{8}m/s) and σ is The Boltzmann constant (5.67*10^{-8}Wm^{-2}k-4=1.38*10^{-23}J/k)

3.5.8.2.1. Split Window Algorithm

The split window algorithm uses different absorption between two thermal infrared channels within one atmospheric window to eliminate the atmospheric influence and calculates surface temperature as a linear combination of two brightness temperatures (Dash *et al*., 2002). The algorithm assumes that the LSE values in both thermal infrared channels are known (Jin *et al*., 2015). This algorithm is functional for sensor where there is two thermal infrared channel, for instance, OLI in Landsat-8 (TIRS band 10 and 11), which was used by (Du *et al*., 2014, Jiménez-Muñoz *et al*., 2014, Jin *et al*., 2015, Qin *et al*., 2001, Rozenstein *et al*., 2014). The general algorithm of the split window can be expressed as:

$$\mathrm{Ts} = \mathrm{TB10} + \mathrm{D1}(\mathrm{TB10} - \mathrm{TB11}) + \mathrm{D2}(\mathrm{TB10} - \mathrm{TB11})^2 + \mathrm{D0} + (\mathrm{D3} + \mathrm{D4W})(1 - \varepsilon) + (\mathrm{D5} + \mathrm{D6W})\Delta\varepsilon \ldots\ldots (17)$$

Where; Ts is Land Surface Temperature, D0 up to D6 =Split Window Coefficient Value, TB10 is the brightness temperature of band 10, TB11is brightness temperature of band 11, and ε is the mean land surface emissivity of thermal infrared bands (mean of band 10 and band 11), W is atmospheric water vapor content and $\Delta\varepsilon$ is Difference in LSE of band 10&11.

Table 3.7: Constant value of a split algorithm

Constants	D0	D1	D2	D3	D4	D5	D6
Value	-0.268	1.378	0.138	54.3	-2.238	-129.2	16.4

According to (Wang *et al*., 2015), the water vapor content of the atmosphere from the first layer to the altitude of the satellite can be determined as follows:

$$w = \frac{w0}{w1} \quad \text{(18)}$$

Where; w is the total water vapor of the atmosphere from the first layer to the altitude of the satellite, w0 is the water vapor of the ground and w1 is the ratio of water vapor content at the first layer to the altitude of the satellite.

The value of w1differ in different atmospheres, with w1= 0.6834 for tropical atmosphere, w1 = 0.6819 and w1 = 0.6593 for subtropical summer and winter atmospheres, respectively, and w1 = 0.6834 and w1 = 0.6356 for mid-latitude summer and winter atmospheres, respectively (Qin *et al*., 2001). Since the study area is found in a tropical atmosphere, the value of w1 is 0.6834. The water vapor content of the ground also can be computed as follows:

$$w0 = {}^{H * B * D}/_{100} \quad \text{(19)}$$

Where, H is air humidity (%) at the ground from meteorology station, B is the saturation mix ratio (g/kg) and D is air density (g/m^3) at specific air temperature. The values of saturation mix ratio and air density at specific air temperature were provided in table 3.7.

Table 3.8: The values of saturation mix ratio and air density at specific air temperature

T (°C)	45	40	35	30	25	20	15	10	5	0	-5	-10
b (g·kg−1)	66.33	49.81	37.25	27.69	20.44	14.95	10.83	7.76	5.5	3.84	2.52	1.63
d (kg·m−3)	1.11	1.13	1.15	1.17	1.18	1.21	1.23	1.25	1.3	1.29	1.32	1.34

Finally, Land surface temperature computed from Landsat TM and OLI/TIRS was converted into degree Celsius, by subtracting 273.15. Therefore, to convert temperature in degree Kelvin to degree Celsius equation 3.17 was used.

$$℃ = K - 273.15 \quad \ldots\ldots (20)$$

Where: ℃: LST in degree Celsius; K: LST in degree Kelvin

3.5.9. Validation of Land Surface Temperature

The results of LST extracted from the thermal band of Landsat 5 TM and Landsat 8 OLI/TIRS images of the study area for the study periods were validated using MODIS data that acquired during a similar period. The MODIS LST and emissivity product at 1km spatial resolution and 8-day temporal resolution retrieved in the Hierarchical Data Format, which is accessed from the NASA Land Process Distributed Active Archive Center (NASA LP DAAC) website (https://earthdata.nasa.gov/about/daacs/daac-lpdaac). The LST of the study area for 2018 has been derived from MOD11A2. The DN value of LST is converted to degree Celsius by using the following formula with the scale factor of 0.02 (Wan, 2013)

$$\mathrm{LST} = (\mathrm{DN} * 0.02) - 273.15 \quad \ldots (21)$$

The validation was carried out based on the ranges and pixel to pixel comparison (Pearson correlation) of the two images' of land surface temperature in this study. But, the spatial resolution of the two images is different and difficult to compare using pixel to pixel comparison. Therefore, the resolution of these two images resamples to 400 m in this study using the nearest resampling technique. Finally, convert pixel values (raster) to point (vector) and extract the values of these points in the ArcGIS environment using extract multi-value to points.

3.5.10. Zonal Statistics

A zone is all the pixels in a raster that have the same value. Zonal statistics are used to calculate statistics for each zone of a dataset based on values from another dataset, a value raster. It divides the raster data based on the zone and calculates statistics for the raster data in the same zone, the cells in the same zone was assigned the same value and output to a new raster dataset (Abel, 2018). A single output value was computed for each cell in each zone defined by the input zone dataset. To analyze NDVI, NDBI, and LST and to understand their spatial distribution in

each LULC type and their variation, zonal statistics were applied in ArcGIS 10.4 software. Urban LULC, NDVI, NDVI, and LST maps were prepared for the years 1988, 2002, and 2018 and statistics were generated. Therefore, to analyze the spatial distribution and temporal variation of LST in each LULC and analyze the impacts of LULC change on LST data was summarized using MS Excel 2016.

3.5.11. Zonation for spatial coverage of LST

The surface temperature was classified into three temperature categories such as low, medium, and high-temperature categories by using minimum, maximum, mean, and standard deviation to see the spatial distribution of LST. Each zone was identified using a pair of temperature thresholds that were determined based on the minimum, maximum, and mean temperatures of the study area (including all LULC types) and its standard deviation. The range of the medium zone was determined by adding the standard deviation from the mean and subtracting the standard deviation to the mean. Therefore, the minimum value of the medium zone was obtained as standard deviation minus the mean, and its maximum value was determined by standard deviation plus the mean temperature of the study area for a specific year. The minimum temperature of the study area for a specific year and minimum value of the medium zone were used to determine the range of low zone, while the maximum value of the medium zone and the maximum temperature of the study area was the range of high zone (Wei *et al*., 2015).

3.5.12. Correlational Analysis

Pearson correlation was used to test the strength of the linear relationship of NDBI and NDVI, with LST for each pixel. It is a measure of the linear relationship between two variables X and Y, giving value range from +1 to -1, where +1 indicates a perfect positive relationship, -1 indicates a perfect negative relationship and 0 indicates no relationship exists (Guo *et al*., 2014). To analyzed the degree of the relationship between the LST and LULC indices (NDVI and NDBI), the value of Pearson correlation coefficient was group based on the absolute value of the correlation coefficients into a weak correlation ($0 < |r| \leq 0.3$), a low correlation ($0.3 < |r| \leq 0.5$), a moderate correlation ($0.5 < |r| \leq 0.8$), and a strong correlation ($0.8 < |r| \leq 1$) (Li *et al*., 2004). The mathematical equation of the Pearson correlation coefficient is presented as follows.

$$r_{xy} = \frac{\sum_{i=1}^{n}(xi-xj)*(yi-yj)}{\sqrt{\sum_{i=1}^{n}(xi-xj)^2 \sum_{i=1}^{n}(yi-yj)^2}} \quad \text{.....(22)}$$

Where, r_{xy} is the simple correlation coefficient of variables X and Y, xi is NDBI, and NDVI of the i^{th} year, Yi is LST of the i^{th} year; Xm is the average NDVI and NDBI for all years, Ym is LST for all years.

CHAPTER FOUR

4. RESULT AND DISCUSSION

The magnitude of LULC, changes, and transformation from 1988 - 2018 was described in this chapter. The results of NDBI, NDVI, the magnitude and spatial coverage of LST, the validation of LST, and the correlation of LST and LULC indices (NDBI and NDVI) for each study period were also included. Besides, the finding of this thesis with other studies that were carried out before in related topics were discussed.

4.1. Accuracy Assessment

The accuracy assessment results of LULC shows that overall accuracy of classification was 88.80%, 91.2%, and 91.6% for the year 1988, 2002, and 2018, respectively. The classification Kappa statistics for 1988, 2002 and 2018 are 86%, 89% and 89.5% respectively. The producers, user accuracy, and kappa statistics results of image classification are provided below in Table 4.1.

Table 4.1: The procedure, user, overall accuracy, and kappa statistics of image classification.

	1988		2002		2018	
Class Name	Producer accuracy in %	User accuracy in %	Producer accuracy in %	User accuracy in %	Producer accuracy in %	User accuracy in %
WB	96	100	94	100	92	100
BL	80	81.63	88	86.24	84	91.3
BU	92	93.88	92	90.2	98	94.23
AG	92	75.41	90	84.91	90	80.04
VE	84	97.67	92	95.83	94	94
OA	88.8		91.2		91.6	
Kappa	86		89		89.5	

Where: WB- water body, BL-bare land, BU-built-up, AG-agriculture, VE- vegetation and OA-overall accuracy

4.2. The Magnitude of Land Use Land Cover in 1988, 2002 and 2018

The supervised classification maximum likelihood was applied to generate the LULC map in 1988, 2002, and 2018 with high accuracy as seen in Table 4.2 and figure 4.1. The dominant LULC classes of 1988 classification were agricultural land and vegetation in the study area. These two classes accounted for 27,237.69 ha (92.23%) of total area coverage. From a total area of 29,237.10 ha, agriculture covered 21,745.8ha (73.45%), and vegetation cover 5491.89 ha (18.78%). The other LULC classes, the bare land, built-up or urban and water body together accounted for 2269.41ha (7.77%) of the total area. The water bodies covered the smallest area than all other classes. The LULC result of 2002 also showed that agriculture covers the largest proportion of land in and around Gondar town with a value of 22103.87 ha (75.6%), followed by vegetation, which covered 40007.79 ha (13.71%). The other LULC classes such as bare land, built-up or urban, and water body together cover 3125.78 ha (10.69%) of the total area. In 2002, also the water body covers the smallest area than all other classes. In 2018, LULC classification results of the study area revealed that the dominant LULC categories were built-up or urban and agricultural land together accounted for 83.77% of total area coverage. From this, agriculture land accounted for 20743 ha (70.95%) and built-up or urban area accounted for 3747.79 ha (12.82%). The remaining LULC classes were bare land, vegetation, and water body together accounted for 16.23% of the total area. However, the extent of agricultural land within the study period decreased by 2.5% from 1988 to 2018. In general, Agriculture is the dominant LULC of the study area concerning area coverage in all the study periods (1988, 2002, and 2018), followed by vegetation in 2002 and built-up or urban area in 2018. A description of statistical data for each class and the LULC map in and around Gondar are shown in Table 4.2 and Figure 4.1.

Table 4.2: The magnitude of LULC in 1988, 2002, and 2018.

No	LULC class	1988		2002		2018	
		Area in ha	Area in %	Area in ha	Area in %	Area in ha	Area in %
1.	Water body	108.24	0.37	148.35	0.51	126.61	0.43
2.	Bare land	1,328.85	4.55	1293.64	4.42	1259.46	4.31
3.	Built-up or urban	832.32	2.85	1683.79	5.76	3747.79	12.82
4.	Agriculture	21,475.80	73.45	22103.87	75.60	20743	70.95
5.	Vegetation	5,491.89	18.78	4007.45	13.71	3360.24	11.49

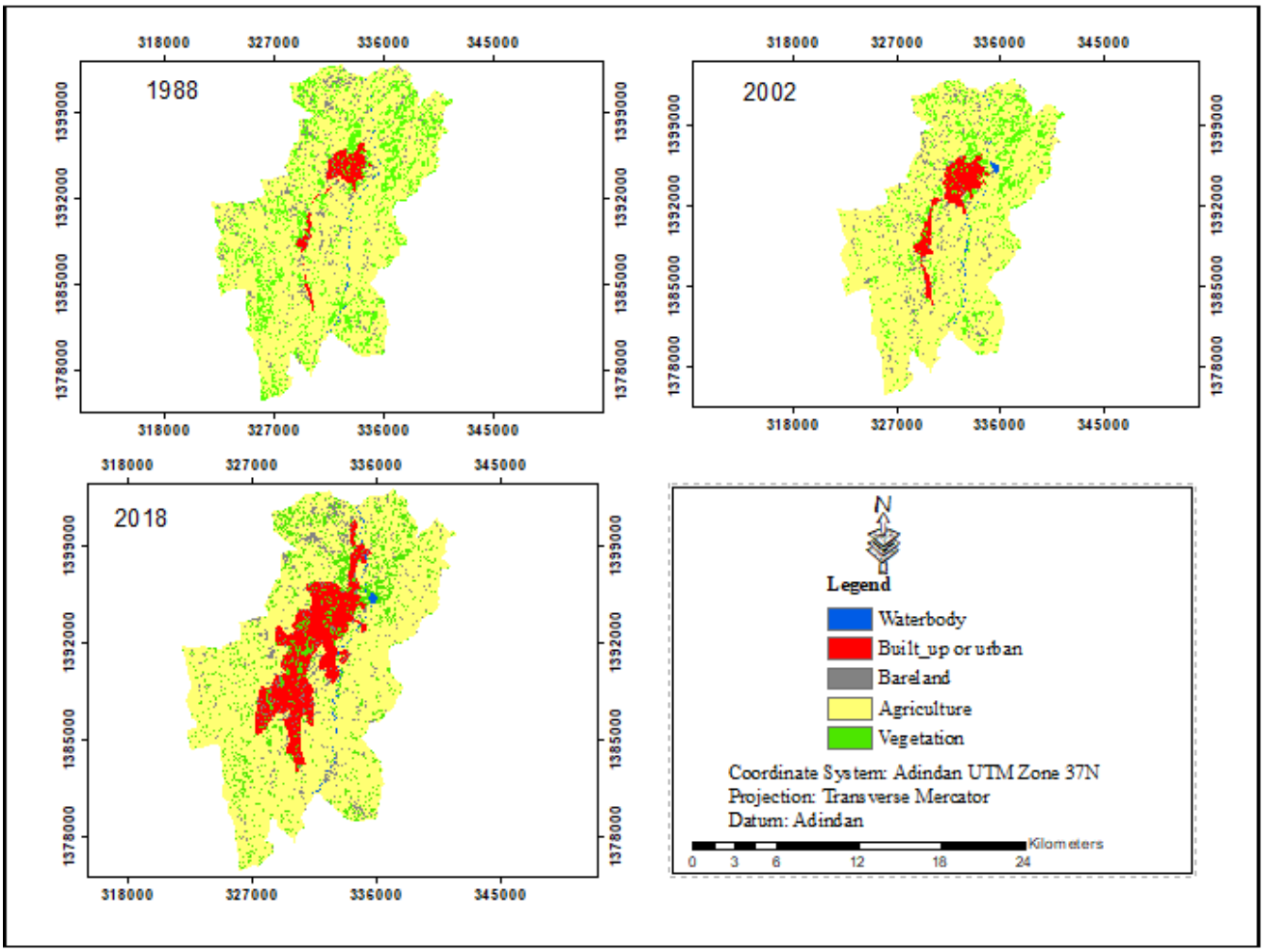

Figure 4.1: LULC class maps of in and around Gondar town 1988, 2002, and 2018.

Agricultural land had the largest spatial extent of all LULC in and around Gondar town from (1988-2018). The extent of agricultural land increased from 21475.8ha to 22103.87 ha in 2002 but it was decreased to 20743 ha in 2018 from 2002 (Figure 4.2).

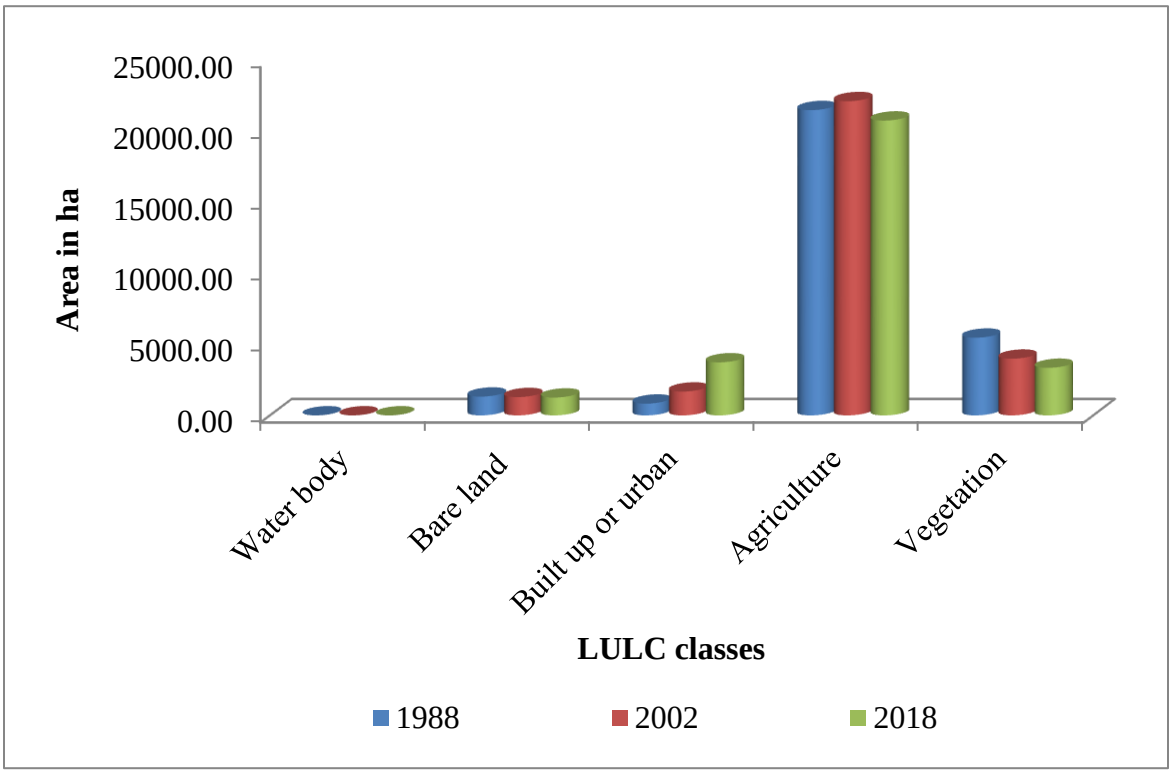

Figure 4.2**:** Temporal LULC distribution and changes in and around Gondar from 1988 - 2018.

4.3. Spatial and temporal changes of LULC

The LULC classification result shows that there was a change in the pattern of LULC in and around Gondar town from 1988 to 2018. From the total LULC classes, more than half of Gondar town was agriculture. However, it has reduced from 21,475.8 ha (73.45%) by 1988 to 20,743 ha (70.95%) in 2018, even if it was increased from 21,475.8 ha in1988 to 22,103.87 ha in 2002.

Vegetation had also decreased from 5,491.89 ha (18.78%) in 1988 to 4007.45 ha (13.71%) in 2002 and reached to 3,360.24 ha (11.49%) in 2018. Similarly, the spatial extent of bare land declined from 1328.85 ha (7.18%) in the initial study year 1988 to 1293.64 ha (4.55%) in 2002 and 1,259.46 ha (4.31%) in 2018.

However, the landscape covered with built-up or urban has increased from 1988-2018. It increased from 832.32 ha (2.85 %,) in 1988 to 1683.79 ha (5.76%) in 2002 and 3747.79 ha

(12.82%), in 2018. The water body was another LULC class in Gondar town that shows some fluctuation from 1988 to 2018. It was 108.24 ha (0.37%) in 1988 and this has increased to 148.35 ha (0.51%) in 2002 due to the construction of the Angereb dam and decreased from 148.35 ha (0.51%) by 2002 to 126.61 ha (0.43%) in 2018. Generally, agriculture, vegetation, and bare land LULC classes were decreased from 1988 - 2018. Whereas, built-up or urban and water bodies were increased through the study period. The description of the Spatio-temporal LUCL change of Gondar town is provided in Table 4.3.

Table 4.3: LULC changes in Gondar town from 1988-2018.

No	LULC class	1988	2002	2018	Net change 1988-2002 in ha	Net change 1988-2002 in %	Net change 2002-2018 In ha	Net change 2002-2018 in %	Net change 1988-2018 in ha	Net change 1988-2018 in %
		Area in ha	Area in ha	Area in ha						
1	WB	108.24	148.35	126.61	40.11	0.14	-21.74	-0.08	18.37	0.06
2	BL	1,328.85	1293.64	1,259.46	-35.64	-0.13	-34.18	-0.11	-69.39	-0.24
3	BU	832.32	1,683.79	3,747.79	851.47	2.91	2,064	7.06	2,915.47	9.97
4	AG	21,475.8	22,103.87	20,743	628.07	2.15	-1360.87	-4.65	-732.8	-2.5
5	VE	5,491.89	4,007.45	3,360.24	-1484.44	-5.07	-647.21	-5.21	-2,131.65	-7.29

Where:- WB-water body, BL- bare land, built-up or urban, AG- agriculture and VE- vegetation

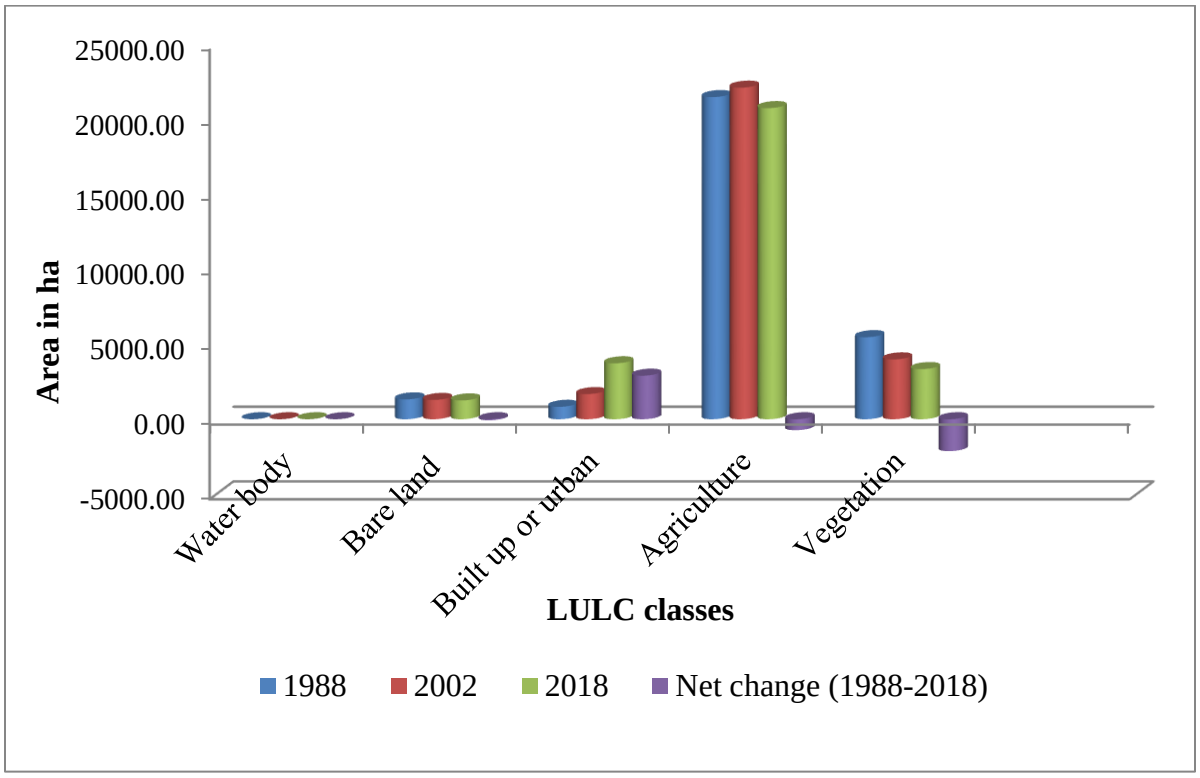

Figure 4.3: LULC changes in 1988, 2002, and 2018.

The LULC transformation matrix from 1988 - 2002 provided in Table 4.4 indicates that the vegetation land in 1988 converted into agricultural land, built-up and bare land in 2002. The major vegetation transformation was made by the expansion of agricultural land (1615.87 ha) and built-up or urban (146.98 ha). In contrary to this, 301.95 ha vegetation areas were gained from bare land and agriculture in 2002. Agricultural land in 1988 also had changed to built-up (urban), vegetation, and bare land by 562.85 ha, 258.27 ha, and 239.72 ha correspondingly. In the same manner, bare land was converted to vegetation, agricultural land, and built-up or urban by 43.68 ha, 111.76 ha, and 151.90 ha in 2002, respectively. Besides, the water body received 38.71ha from agriculture in 2002 due to the construction of the Angereb dam. The built-up or urban areas also received 146.68ha, 151.90ha, and 562.85ha from vegetation, bare land, and agricultural land respectively. The details of the LULC transformation matrix from 1988-2002 are presents in Table 4.4.

Table 4.4: The LULC transformation matrix of Gondar town from 1988-2002 in ha.

	LULC classes	LULC_1988					
		WB	AG	BL	VG	BU	RT
LULC_2002	WB	**108.00**	38.71	0.78	0.86	0	148.35
	AG	0	**20376.23**	111.76	1615.87	0	22103.87
	BL	0.24	239.72	**1020.73**	22.98	9.96	1293.64
	VG	0	258.27	43.68	**3705.50**	0	4007.45
	BU	0	562.85	151.90	146.68	**822.36**	1683.79
	CT	108.24	21475.80	1328.85	5491.89	832.32	29237.10

Where: WB-water body, AG- agriculture, BL- bare land, VG-vegetation, BU-built-up or urban, CT-column total, and RT- row total.

Based on the LULC transformation matrix from 2002-2018 in table 4.5, from a total area of vegetation in 2002, 720.74 ha, 95.72 ha, 48.95 ha were correspondingly converted to agricultural land, built-up or urban, and bare land in 2018. During this period (2002-2018), agriculture was also converted into vegetation, built-up(urban), and bare land. Additionally, areas classified as bare land in the year 2002 changed to agriculture (70.09 ha), vegetation (55.68 ha), and built-up or urban (116.95 ha) in 2018. In the same period, 22.35 ha of water bodies were changed to vegetation.

Table 4.5: The LULC transformation matrix of Gondar town from 2002-2018 in ha.

	LULC classes	LULC_2002					
		WB	BU	BL	AG	VG	RT
LULC_2018	WB	**126.00**	0	0	0.41	0.20	126.61
	BU	0	**1662.91**	116.95	1872.21	95.72	3747.79
	BL	0	13.13	**1050.92**	146.46	48.95	1259.46
	AG	0	7.75	70.09	**19944.43**	720.74	20743.00
	VG	22.35	0	55.68	140.36	**3141.85**	3360.24
	CT	148.35	1683.79	1293.64	22103.87	4007.45	29237.10

Where: WB-water body, VE- vegetation, BL-bare land, Built-up or urban, AG-agriculture, CT-column total, and RT-row total.

Additionally, bare land in 2018 was reduced due to the expansion of agricultural land, built-up or urban and vegetation. From 2002 - 2018, vegetation was converted to agriculture, built-up (urban), and bare land. In this period, areas covered by the water body were also converted to agriculture and vegetation. The LULC transformation matrix of Gondar town from 1988 - 2018 is presented in Table 4.6.

Table 4.6: The LULC transformation matrix of Gondar town from 1988 – 2018 in ha.

	LULC classes	LULC-1988					
		WB	BU	BL	AG	VG	RT
LULC_2018	WB	**107.96**	0	7.00	10.80	0.85	126.61
	BU	0	**821.63**	132.62	2488.99	304.56	3747.79
	BL	0.28	0.00	**1118.52**	63.22	77.44	1259.46
	AG	0	4.35	65.89	**18824.25**	1848.50	20743.00
	VG	0	6.34	4.82	88.54	**3260.54**	3360.24
	CT	108.24	832.32	1328.85	21475.80	5491.89	29237.10

Where: WB-water body, VE- vegetation, bare land, Built-up or urban, AG-agriculture, CT- class total.

4.4. The Spatio-temporal Distribution of NDVI

Based on NDVI results, extracted from near-infrared and red bands within the study periods show that LULC classes have different NDVI values. The value varies from area to area based on vegetation intensity and condition. Vegetation cover has the highest NDVI value than other classes. The spatial extent of vegetation cover in 1988 was greater than in 2002 and 2018 in and around Gondar town. Since the NDVI value was higher in 1988 with its mean of 0.190 than in 2002 and 2018 which were 0.0183 and 0.0.145 respectively. This shows that there was high vegetation cover in 1988 than in 2002 and 2018 (Table 4.7).

Table 4.7: The NDVI values for 1988, 2002 and 2018

Year	Maximum	Mean	Minimum	Standard Deviation
1988	0.695	0.190	-0.450	0.063
2002	0.647	0.183	-0.385	0.090
2018	0.541	0.145	-0.084	0.090

Figure 4.4 shows the place that has the highest NDVI value corresponds to vegetation cover mostly in the northeast, east, northwest, west, south, and central parts of the town mainly around the Mintwab Lodge, University of Gondar, Kusqam, and Debre Birhan church, whereas the area covered by built-up, agriculture, bare land, and water body has low NDVI values.

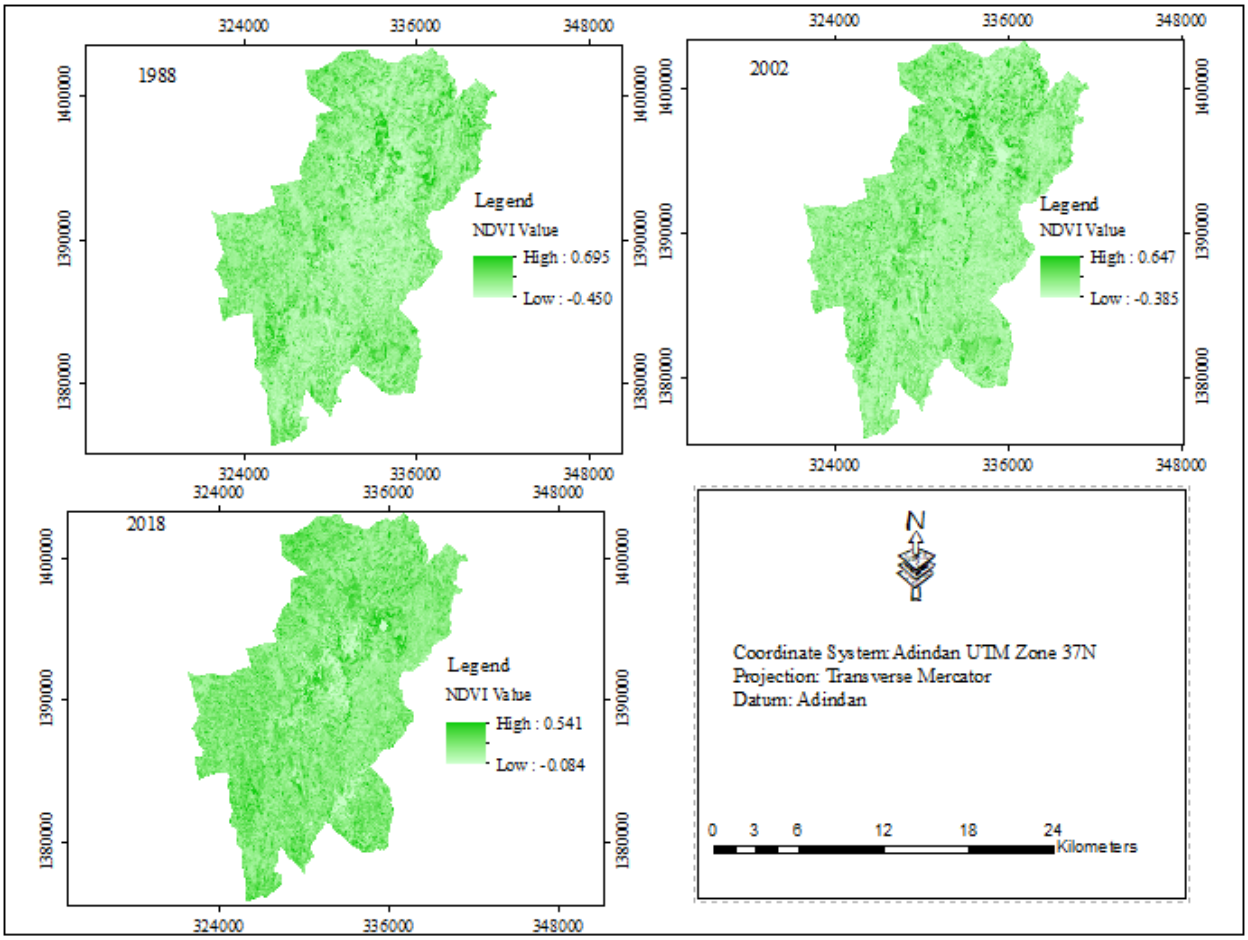

Figure 4.4: NDVI map of in and around Gondar for the year 1988, 2002 and 2018

4.5. The Spatio-temporal Distribution of NDBI

The distribution of NDBI value in figure 4.5 shows an opposite design to the NDVI maps in the sense that vegetation covers high NDVI values and received low NDBI values. Likewise, an urban or built-up area is characterized by low NDVI and high NDBI values. The lowest NDBI was computed from water bodies while the highest values were possessed by agriculture land, bare land, and urban (built-up) area. In general, the built-up or urban areas have higher reflectance to the short wave Infrared band and it was expected to have higher NDBI (Malik et

al., 2019). It is observed that higher NDBI values correspond to urban (built-up), bare land, and agriculture areas in the central, east, and west parts of a town, while lower values were observed in water bodies and vegetation areas. The NDBI values of the town ranged from -0.75 to 0.63 in 1988, -0.41 to 0.24 in 2002, and -0.44 to 0.48 in 2018.

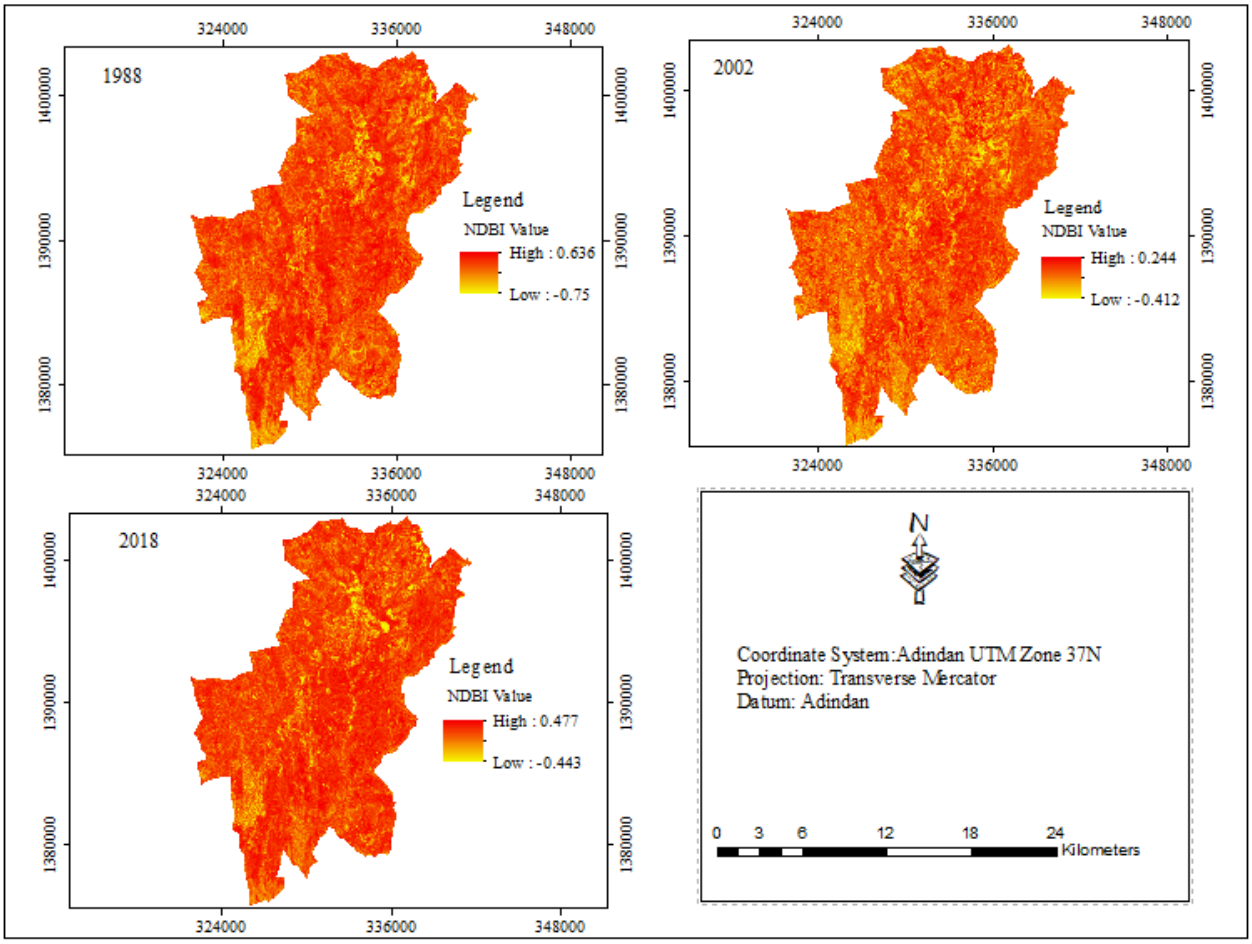

Figure 4.5: NDBI map of in and around Gondar town for the year 1988, 2002 and 2018

4.6. The Spatio-temporal Distribution of LST from 1988-2018

According to the results produced by the researcher, the calculated values of the LST for the year 1988 ranged from 13.44 ^{0}C - 36.84 ^{0}C, with the mean values of, 27.04 ^{0}C. For the year 2002, it ranged from 15.46 ^{0}C to 38.25 ^{0}C, with the mean value of 28.46 ^{0}C while in 2018 it ranged from 16.14 - 41.32 ^{0}C, with the mean value of 29.86 ^{0}C. The mean temperature increased by 1.42 ^{0}C from 1988 to 2002 and 1.40 ^{0}C from 2002 to 2018. The mean LST was increased sharply by 2.82 ^{0}C from 1988 to 2018. Areas denoted by an oval shape and the like had a high temperature.

Most of those areas were covered by bare land, agriculture, and built up which was exposed directly to incoming radiation. The areas denoted by a rectangle and the like had a low temperature, which is covered with vegetation. The distribution of LST of Gondar town for 1988 is presented in figure 4.6.

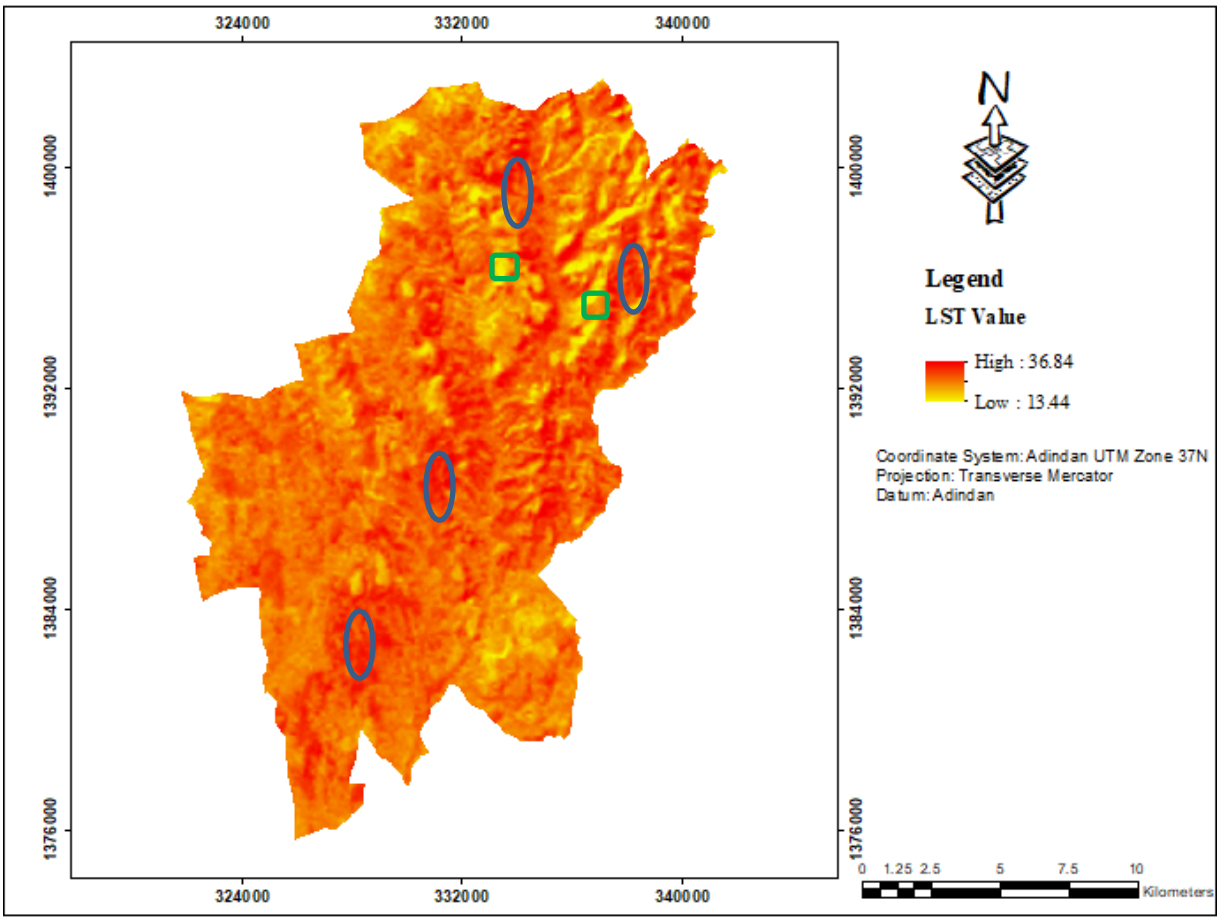

Figure 4.6: LST map of in and around Gondar town for the year 1988.

The spatial extent of LST in 2002 was higher than the year 1988 with its maximum value of 38.25 ℃ in Gondar town. These areas were found in areas denoted by an oval shape and the like. However, some places covered with vegetation and water have a low temperature which is denoted by a small rectangle and the like. The distribution of LST of Gondar town for 2002 is presented in figure 4.7.

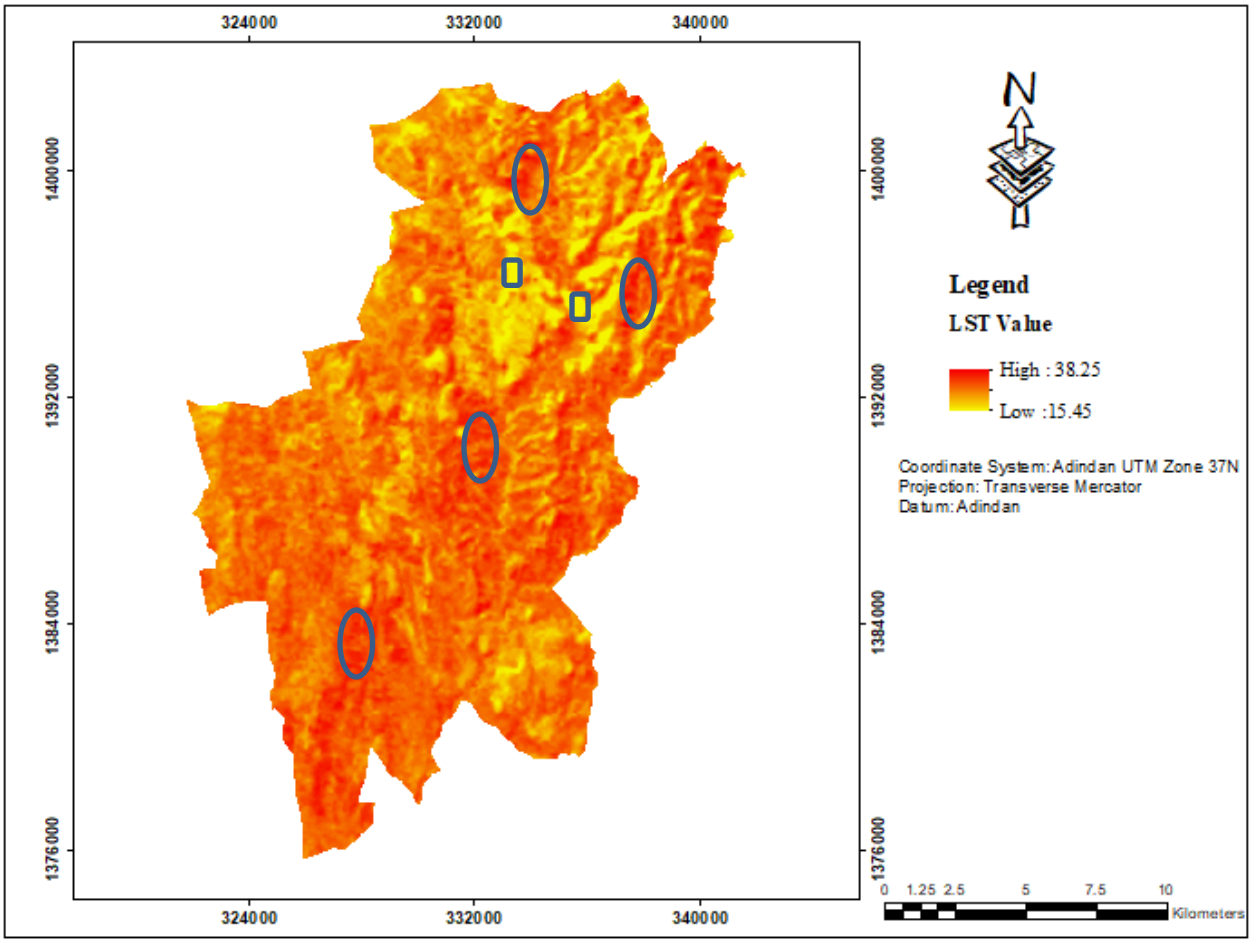

Figure 4.7: LST map of in and around Gondar town in 2002.

The LST map of Gondar town in 2018 shows that still the places that are denoted by oval shape had a high LST and the places that are denoted by small rectangle had a low LST. However, the spatial extent of high LST expanded into the central part of the town, and the places that built-up or urban areas expanded because the pattern of built-up in the year 2018 is denser than in 1988 and 2002. The distribution of LST of Gondar town for 2018 is presented in figure 4.8.

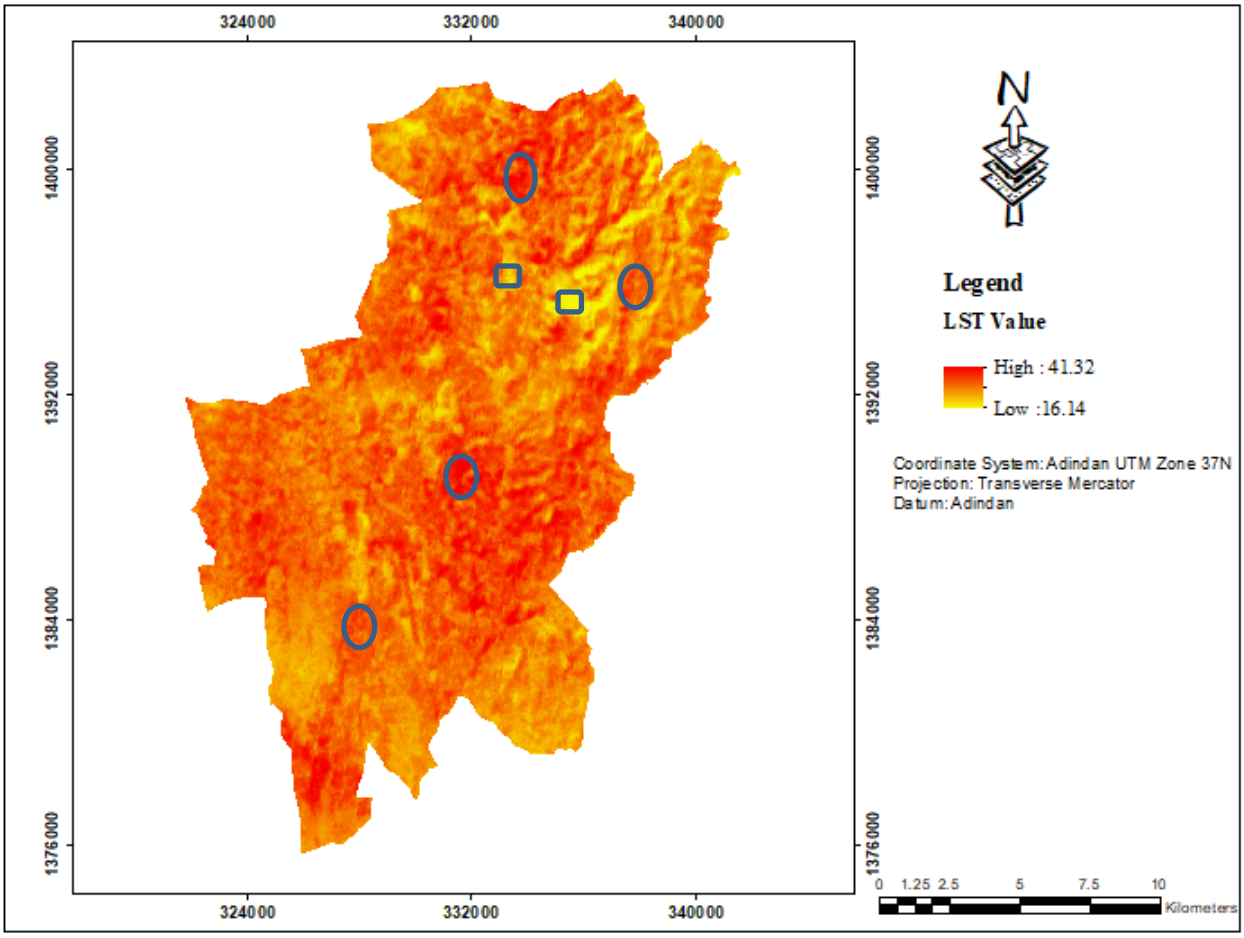

Figure 4.8: LST map of in and around Gondar town for the year 2018

4.7. Validation of LST Derived from Landsat Thermal Band

In this study, MODIS data were used to validate the Landsat eight LST of Gondar town in 2018 that were acquired during a similar period, even if, MODIS has a coarser resolution. The LST result derived from MODIS and Ladsat8 ranges from 19.95℃ to 41.67℃ and 16.14℃ to 41.32℃ respectively. Central, eastern, southern and western part of the town in most places has a high temperature in both sensors. Whereas, the northern part of the town and places around Angereb dam has a low temperature in both sensors. Therefore, the ranges of LST extracted from both sensors in and around Gondar town were close to each other.

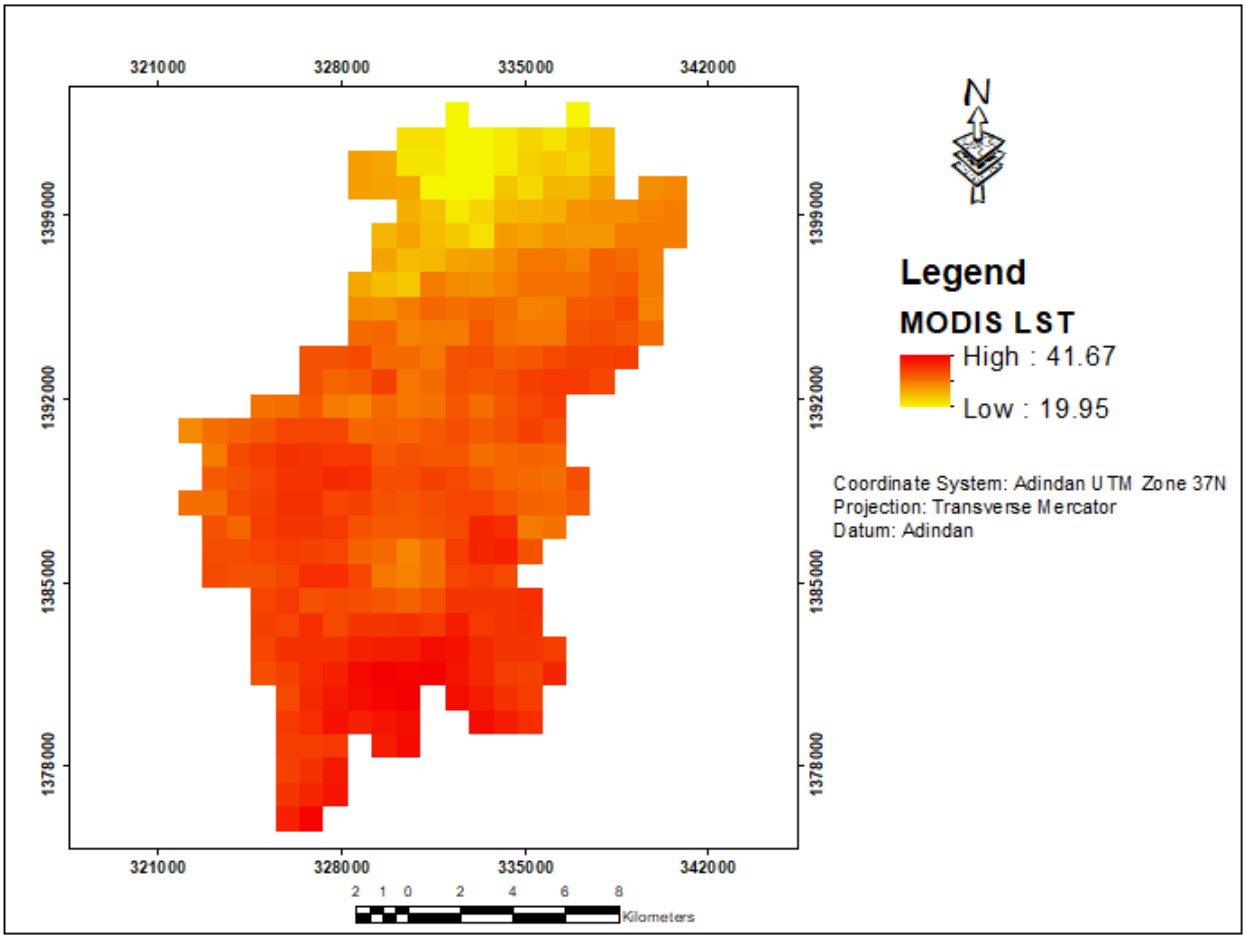

Figure 4.9: MODIS LST data used to validate LST extracted from Landsat

The scatter diagram of Landsat and MODIS LST also shows a moderate positive relationship with a coefficient of determination (R^2) and Pearson correlation coefficient (r) are 0.3 and 0.55 respectively. This indicates the value of LST of Landsat increases the values of MODIS LST also increases.

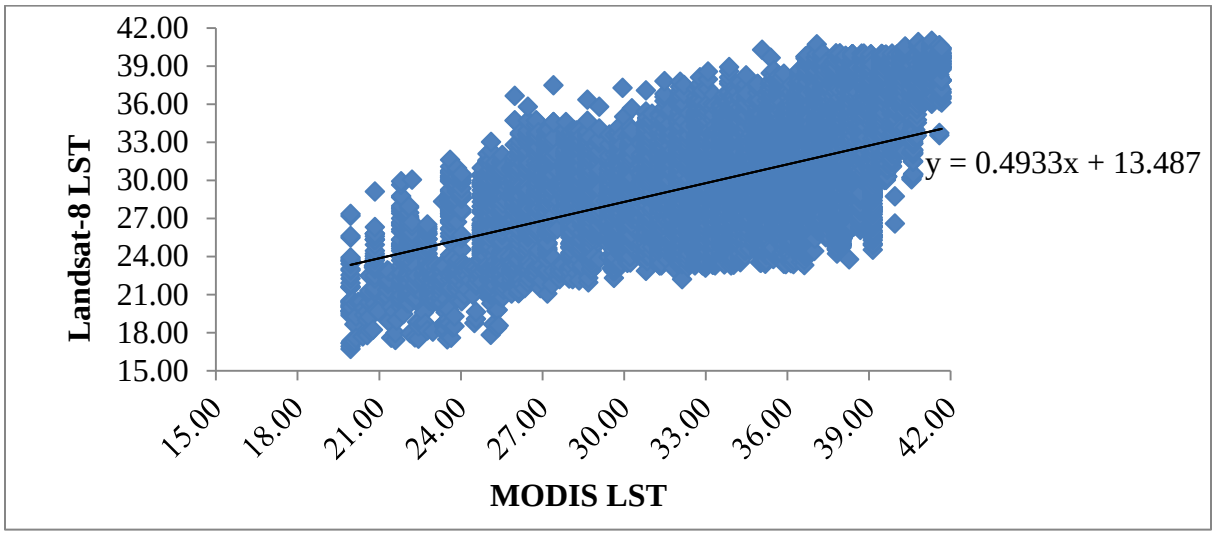

Figure 4.10: Scatter plot of the MODIS and Landsat LST.

4.8.The spatial coverage of LST and Distribution in 1988, 2002 and 2018

Results in this study show that LST was progressively changed from 1988 - 2018. The range of LST of Gondar town varies from 13.44 ºC - 41.32 ºC. This LST was categorized into three zones such as High, Medium, and Low presented in Table 4.8 and Figure 4.11. In 1988, most of the areas of Gondar town had a medium temperature range from 24.94 ºC - 29.94 ºC, that spatially covered about 16,286 ha. In this year, the low-temperature zone that ranges from 13.44 ºC - 24.94 ºC with spatial coverage of 4552 ha, and the high-temperature zone was covered 8,394 ha with the range of 29.94 ºC - 36.84 ºC. This temperature was changed to 38.25℃ in the year 2002. Therefore, the spatial coverage of high, medium and low zones was 12,079 ha, 12,918 ha, and 4,235 ha respectively. Moreover, larger parts of Gondar town were covered by a high-temperature zone in 2018 because the maximum LST of the town changed to 41.32 ^{0}C. The LST zone and their aerial coverage are tabulated as follows in Table 4.8.

Table 4.8: LST zones and their aerial coverage in 1988, 2002 and 2018

Year	Zone	Range in ^{0}C	Area coverage in ha	Total area in ha
1988	High	29.94-36.84	8394	29237
	Medium	24.94-29.94	16286	
	Low	13.44-24.94	4557	
2002	High	31.44-38.25	12079	29237
	Medium	25.48-31.44	12923	
	Low	15.46-25.48	4235	
2018	High	32.73-41.32	14065	29237
	Medium	26.39-32.73	11812	
	Low	16.14-26.39	3360	

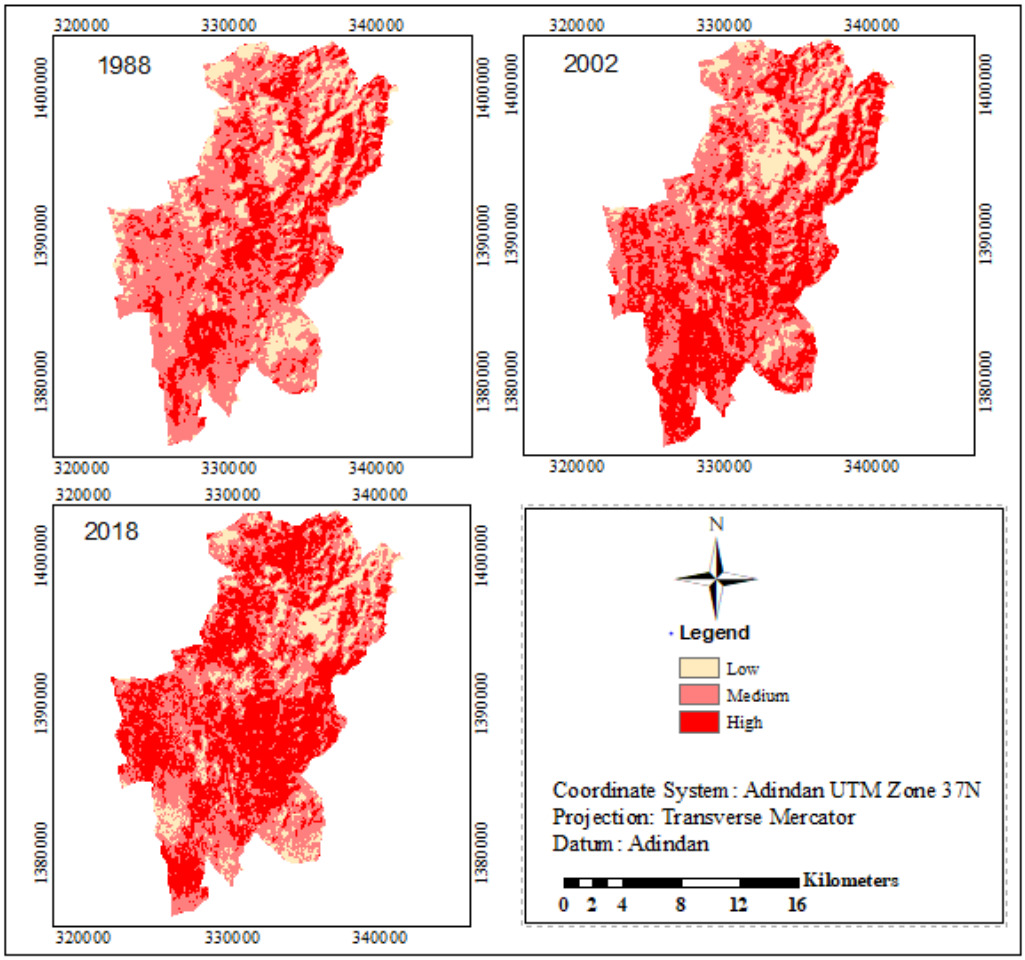

Figure 4.11: LST zone in and around Gondar town

4.9. The Association of Land Surface Temperature with LULC Indices

4.9.1. The Association of land surface temperature with NDVI

This is an index that indicates the health status of vegetation, and the greenness of the earth's surface. So, it is used to assess the urban environment and urban heat island since it shows the level of dryness and warmness of the town. The association between LST and NDVI is negative in 1988, 2002, and 2018 (table 4.9 and figure 4.12). This means Low LST has high NDVI and high LST has low NDVI. This indicates that higher temperature is one reason for the increase of evaporation, and consequently, a lower plant production. The results in this study have similar suggestions with the study done by Lakshmi Kumar *et al*., (2013) on the relationship between temperature and vegetation changes. The higher NDVI has lower LST, the lower NDVI has a higher LST except for the water body. Since the reflectance of a water body in the infrared region is lower than the red spectrum, it emits radiation in the thermal region, LST and NDVI have a positive relationship (Abel, 2018).

The value of coefficient determination of NDVI and LST is 0.68, 0.70, and 0.71in 2018, 2002, and 1988 respectively. Therefore, 68%, 70%, and 71% distribution of LST was influenced by NDVI in 2018, 2002, and 1988 correspondingly without ignoring other factors like topography and elevation. Hence, NDVI is not the only factor for the distribution of LST in Gondar town (Abel, 2018). The results in this study indicate that there was a strong negative association LST with NDVI having a value of Pearson correlation coefficients (r) -0.83, -0.84, and -0.84 for 2018, 2002, and 1988 respectively. Other studies like Sobrino *et al*. (2001); Sun *et al*. (2012); Worku, (2018), and Yue *et al*. (2007) also agreed with a negative association between LST and NDVI. However, the LST values of water bodies increase with the increase of NDVI values because of its large heat emitting capacity in the thermal spectrum. The study conducted by Dong et al. (2018) shown that the LST of water bodies increases with increases of NDVI since the heat capacity of water is relatively large.

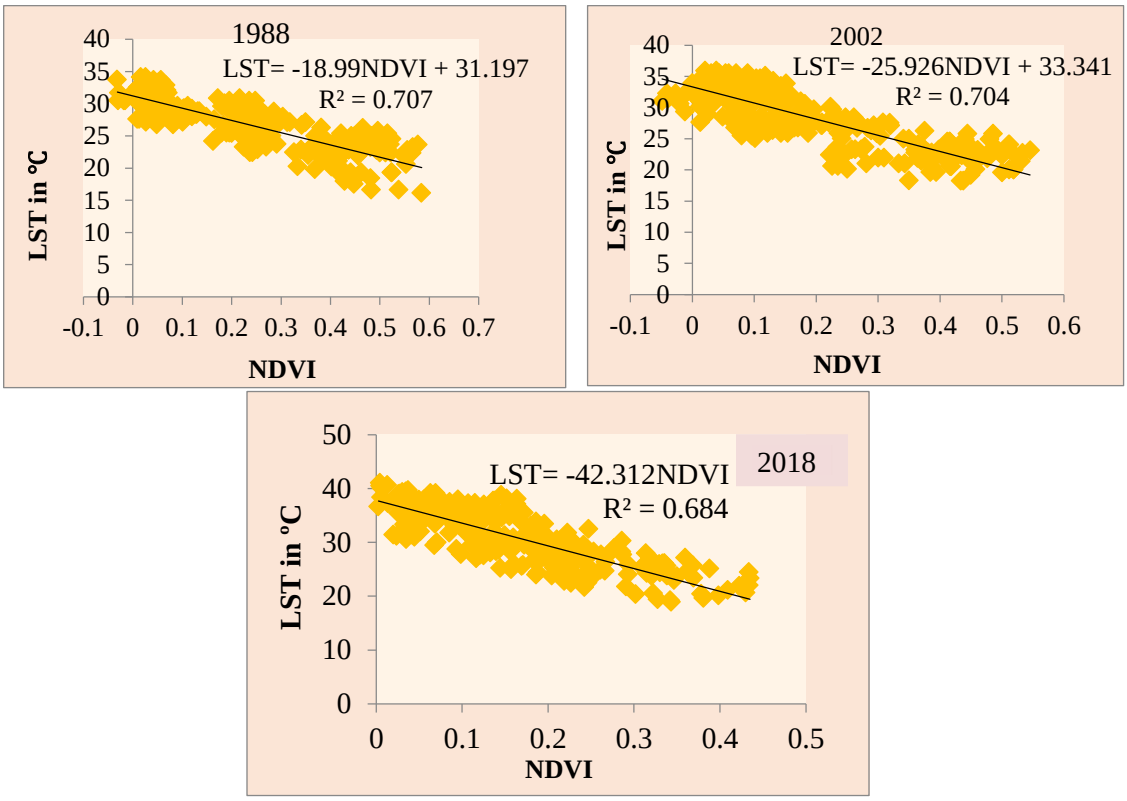

Figure 4.12: Correlation of LST with NDVI for the year 1988, 2002, and 2018.

Table 4.9 Pearson Correlations of LST with NDVI in 1988, 2002, and 2018 with a 5% significance level.

	NDVI			
	Year	R^2	R	Linear equation
LST	1988	0.707	-0.841	LST = -18.99NDVI + 31.197
	2002	0.704	-0.839	LST = - 25.926NDVI + 33.341
	2018	0.684	-0.827	LST = - 42.312NDVI + 37.819

4.9.2. The Association of Land Surface Temperature with NDBI

The result shows that increasing impervious surfaces like asphalt, built-up and parking lots modified thermal behavior and was important to increased NDBI. This arrangement can be seen in Tables 4.10, showing the association of NDBI with Land surface temperature. Therefore, the sign of the coefficient shows whether the correlation is positive or negative. The amount of the correlation indicates the weakness or strength of the correlation. we can describe in words the

degree of the association based on the guide that Li *et al*. (2004) mentioned in chapter three. The results indicate that the association between LST and NDBI is moderately positive in 1988. However, the correlation of LST with NDBI was strongly positive in 2002 and 2018. This indicates low NDBI has low LST and high NDBI has high LST. Generally, the relation of LST and NDBI in this study is positive in all study periods. The results in this study have similar suggestions with the study done by Malik *et al.* (2019) on the relationship between LST with NDBI, and NDVI. The value of the correlation of LST with NDBI was 0. 82, 0.80, and 0.78 in 2018, 2002, and 1988 respectively. It indicates that built-up or urban areas, agriculture, and bare land aggravate the LST in Gondar town because of this land-use classes have high NDBI values (figure 4.13 and table 4.10).

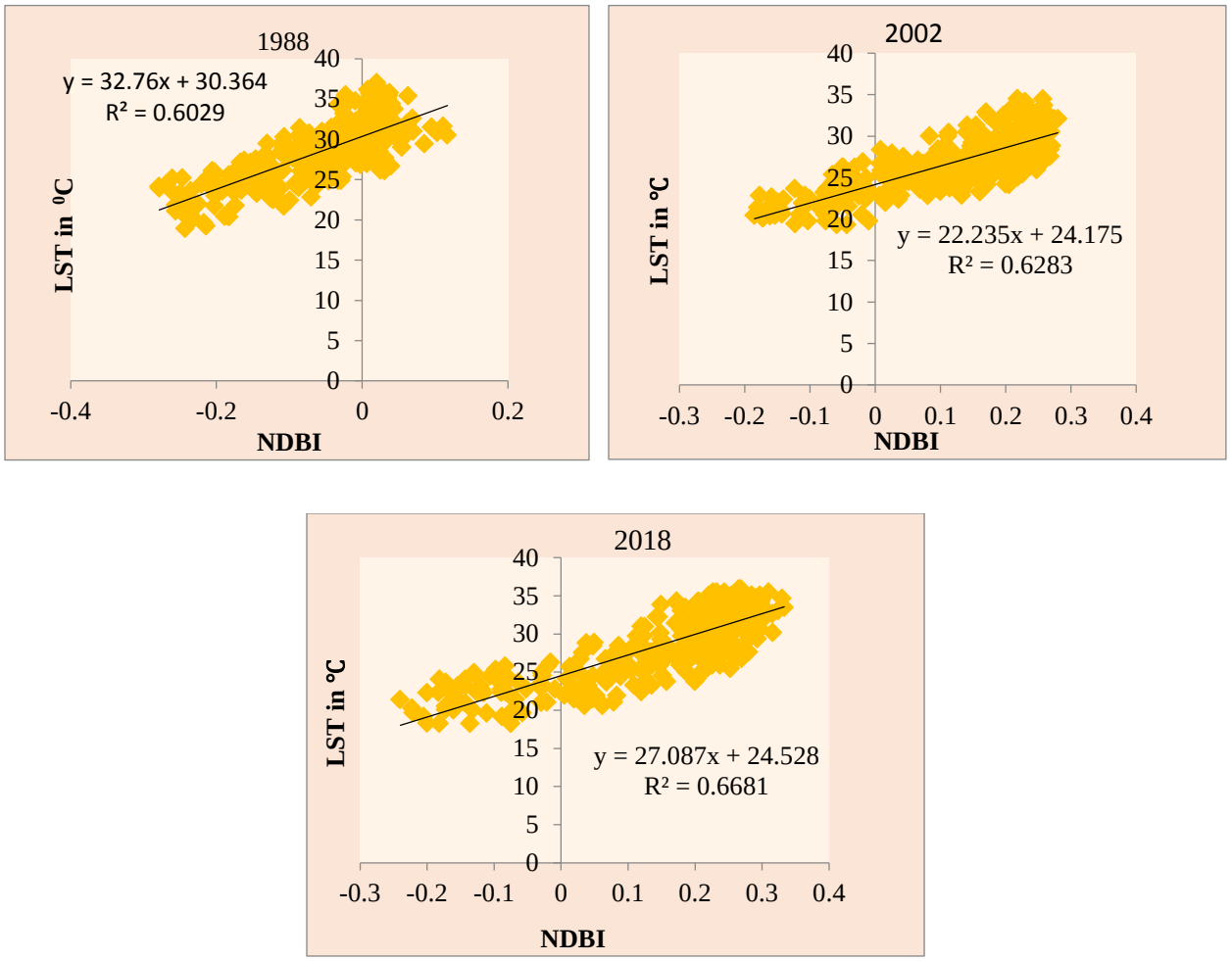

Figure 4.13: correlation of LST with NDBI for the year 1988, 2002, and 2018.

Table 4.10: Pearson Correlations of LST with NDBI in 1988, 2002, and 2018 with a 5% significance level.

	NDBI			
	Year	R^2	r	Linear equation
LST	1988	0.603	0.78	LST = 32.76NDBI + 30.364
	2002	0.628	0.80	LST = 22.235NDBI + 24.175
	2018	0.668	0.82	LST = 27.087NDBI + 24.528

4.10. The Land Surface Temperature Value of Each Land Use and Land Cover

The results in this study illustrate that there was a conversion of vegetation cover to built-up or urban areas, agricultural land, and bare land (Figure 4.1). Mainly, the expansion of built-up in the north, east, southwest, and central part of the town made the area warmer from 1988 - 2018. Such LULC conversion caused the increase in LST in Gondar town.

As presented in table 4.11, agricultural land and bare land recorded higher LST than other land use and land cover. The LST of agricultural land was 36.84 ℃, 38.25 ℃, and 41.32 ℃, and the LST of bare land was 36.05, 37.85, and 41.15 in 1988, 2002, and 2018 respectively. In addition to this, built-up or urban areas also record maximum surface temperatures of 39.45 ℃, 36.66 ℃, and 36.05 ℃ in 2018, 2002, and 1988 respectively (Table 4.10).

The surface temperature of water bodies has been decreasing relatively fast from 28.35℃ to 27.68 ℃ and 27.68 ℃ to 24.35 ℃ in 1988 and 2018 correspondingly. On the other hand, vegetation cover had greater LST than water bodies and lower than the remaining LULC classes. It was 34.02 ℃, 36.22 ℃, and 37.97 ℃ in 1988, 2002, and 2018 respectively. The LST of each LULC class is tabulated in Table 4.11.

Table 4.11: The land surface temperature of Gondar town for each LULC from 1988 - 2018

LULC classes	1988				2002				2018			
	Max	Min	Mean	STD	Max	Min	Mean	STD	Max	Min	Mean	STD
AG	36.84	17.11	27.6	2.45	38.25	17.91	29.67	2.4	41.32	17.09	31.11	2.91
BL	36.05	18.86	29.16	2.58	37.85	22.84	31.75	2.17	41.15	21.47	33.22	2.84
BU	36.05	16.23	26.44	2.9	36.66	18.25	28.62	3.1	39.45	18.69	30.61	2.57
VE	34.02	13.44	24.44	2.78	36.22	15.46	26.71	3.07	37.97	16.14	27.46	2.9
WB	28.35	18.09	20.55	1.87	27.68	16.11	20.09	1.75	24.35	17.09	19.98	0.35

Where: AG-agriculture, BL-bare land, BU-built-up or urban, VE-vegetation, and WB-water body.

4.11. The association of Land Use and Land Cover with Mean Land Surface Temperature change

The map of LULC and LST of Gondar town shows how LULC and LST have changed from 1988 - 2018. This change was mainly due to the high percentage of land transformation. The LST increased from 1988 to 2018 and varied with the variation of LULC. Among the LULC classes, vegetated land and water body regions of the Gondar town had a low LST change and high radiation was emitted by built-up and bare land. From 1988 - 2018, the cumulative mean LST has increased by 2.82 °C (Table 4.12). The mean LST for each LULC class is presented in table 4.12 and Figure 4.14.

Table 4.12: The mean LST changes for each land use and land cover from 1988-2018

LULC classes	Mean LST			LST change		
	1988	2002	2018	1988-2002	2002-2018	1988-2018
Agriculture	27.6	29.67	31.11	2.07	1.44	3.51
Bare land	29.16	31.75	33.22	2.59	1.46	4.05
Built-up or urban	26.44	28.62	30.61	2.18	1.99	4.17
Vegetation	24.44	26.71	27.46	2.27	0.75	3.02
Water body	20.55	20.09	19.98	0.46	-0.11	-0.57

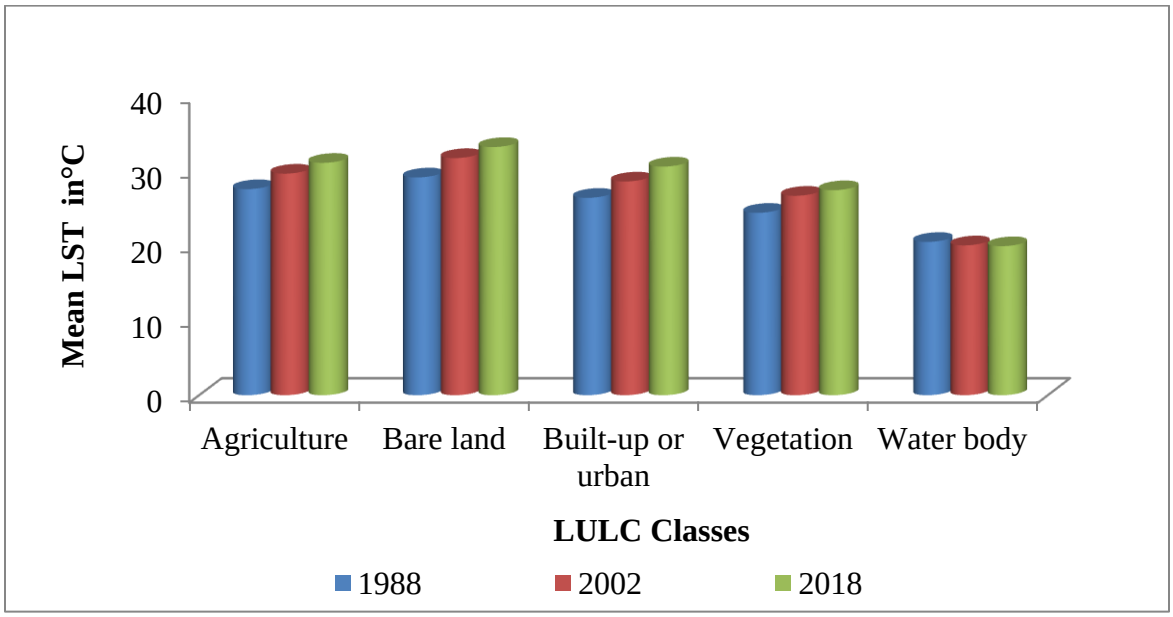

Figure 4.14: The relationship between mean land surface temperatures and each LULC.

CHAPTER FIVE

5. CONCLUSION AND RECOMMENDATION

Under this chapter, the basic finding of this study and suggestions to concerned bodies were described based on the results described in the previous chapter.

5.1. Conclusion

Remotely sensed data is useful for different applications such as LULC change detection, mapping NDVI and NDBI, and environmental management programs. Landsat imageries and MODIS data can examine the LULC changes and to analyze the Spatio-temporal distribution of LST. This study has used Landsat TM5, and Landsat OLI/TIRS images to analyze the impact of LULC changes on LST. Land surface temperature and LULC derived from such imageries give important information to monitor human activities and environmental changes. It was expressed that Landsat images are very useful in quantifying and mapping LULC change, NDVI, NDBI, and LST in Gondar town. The LULC pattern of Gondar town has attributed to socio-economic and natural factors and their exploitation in time and space. Bare land, built-up or urban and agriculture areas have high LST whereas water body and vegetation areas have low LST in the study area. The LULC of Gondar town has been changing through time due to rapid population growth associated with the exploitation of land cover and urbanization. This change has an impact on LST in this study area. For each study period (1988, 2002, and 2018), the minimum and maximum LST value has increased. Therefore, Calculated LST acts an important role or functions of LULC and changes the temperature condition of the area.

Results in this study show that the LST of Gondar town has increased from 1988 - 2018. This was because of LULC changes caused by human activities and climate variability of the area. The LST of the town shows a high variation in LST between different LULC types. Higher LST changes occur in built-up areas and low LST changes occur in the water body through the study period. The LST values derived from Landsat has fine harmony with LST values derived from MODIS data. The NDVI and NDBI values calculated from satellite data also a good indicator of the LST status of the study area. The LST has a positive relationship with the NDBI and it has a negative relationship with the NDVI in the town. Generally, the use of data comes from remote sensing to investigate the variations in LST, and different LULC class patterns in Gondar town

express that it suggests a quicker and cost-effective technique with the advantage of covering a large area.

5.2. Recommendation

Based on the results provided in chapter four, the following recommendations have been forwarded.

- LULC changes are a series problem in and around Gondar town and a central component in current approaches for handling resources and observing environmental changes. Thus, urban land management and environmental protection experts should give high attention to policies and strategies that govern proper and environmental use of land and its cover.
- High temperature is found in agricultural and bare land areas in a town. Therefore, tree plantation should be extended along with the agricultural land and bare land to refresh thermal accumulation effects in the area.
- Places in the center of the town and peripheral built-up areas have higher urban heat islands. So, the concerned bodies consider how to increase tree plantation, green parks, and green roofs in those vulnerable areas.

6. REFERENCES

Abate, S. 2011. Evaluating the land use and land cover dynamics in Borena Woreda of South Wollo Highlands, Ethiopia. *Journal of Sustainable Development in Africa,* 13**,** 87-107.

Abbas, I., Muazu, K. & Ukoje, J. 2010. Mapping land use-land cover and change detection in Kafur local government, Katsina, Nigeria (1995-2008) using remote sensing and GIS. *Research journal of environmental and Earth Sciences,* 2**,** 6-12.

Abel, B. 2018. Impacts of land use and land cover changes on land surface temperature distribution in Bahir Dar town and its surrounding using remote sensing. MSc. Thesis Addis Ababa University, Ethiopia.

Agarwal, C., Green, G., Grove, M., Evans, T. & Schweik, C. 2000. A Review and Assessment of Land-Use Change Models Dynamics of Space, Time, and Human Choice.

Alhawiti, R. H. & Mitsova, D. 2016. Using Landsat-8 data to explore the correlation between urban heat island and urban land uses. *IJRET: International Journal of Research in Engineering Technology,* 5**,** 457-466.

Amare, S. (2015). Land use/cover change at Infraz Watershed, Northwestern Ethiopia. *Journal of Landscape Ecology*, 8(1):69-83.

Anderson, J., Hardy, E., Roach, J. & Witmer, R. 1976. Land use and land cover classification system for use with remote sensor data [USA]. *Professional Papers-US Geological Survey(USA). no. 964.*

Becker, F. & Li, Z.-L. 1990. Towards a local split-window method over land surfaces. *Remote Sensing,* 11**,** 369-393.

Becker, F. & Li, Z. L. 1995. Surface temperature and emissivity at various scales: Definition, measurement, and related problems. Remote Sensing Reviews, 12, 225-253.

Bekele, H. 2005. Urbanization and Urban Sprawl Master of Science Thesis No. 294 Department of Infrastructure Section of Building and Real Estate Economics.

Belay, S., Amsalu, A. & Abebe, E. 2014. Land use and land cover changes in Awash National Park, Ethiopia: impact of decentralization on the use and management of resources. *Open Journal of Ecology,* 4**,** 950.

Brink, A. B., Bodart, C., Brodsky, L., Defourney, P., Ernst, C., Donney, F., Lupi, A. & Tuckova, K. 2014. Anthropogenic pressure in East Africa—Monitoring 20 years of land cover changes using medium resolution satellite data. *International Journal of Applied Earth Observation and Geoinformation,* 28, 60-69.

Central Statistical Agency (CSA). (2015). Population Projection of Ethiopia for All Regions at Wereda Level from 2014 – 2017 (Population projection). The Federal Democratic Republic of Ethiopia Central Statistical Agency, Addis Ababa, Ethiopia.

Central Statistical Agency (CSA). (2007). The 2007 population and housing census of Ethiopia:

statistical reports for the Amhara region (Census report). The Federal Democratic Republic of Ethiopia, Office of population and housing census commission, Central Statistical Agency, Addis Ababa, Ethiopia.

Central Statistical Agency (CSA). (1994). The 1984 population and housing census of Ethiopia:

Analytical report at the national level (Census report). The transitional government of Ethiopia,

Office of the population and housing census commission, Addis Ababa, Ethiopia.

Chander, G., Markham, B. L. & Helder, D. L. 2009. Summary of current radiometric calibration coefficients for Landsat MSS, TM, ETM+, and EO-1 ALI sensors. *Remote sensing of environment,* 113**,** 893-903.

Congalton, R. & Green, K. 2009. Thematic accuracy. *Assessing the Accuracy of Remotely Sensed Data: Principles and Practices***,** 55-61.

Congalton, R. G. 1991. A review of assessing the accuracy of classifications of remotely sensed data. *Remote sensing of environment,* 37**,** 35-46.

Dash, J., Mathur, A., Foody, G. M., Curran, P., Chipman, J. & Lillesand, T. 2007. Land cover classification using multi- temporal MERIS vegetation indices. *International Journal of Remote Sensing,* 28**,** 1137-1159.

Dash, P., Gottsche, F.-M., Olesen, F.-S. & Fischer, H. 2002. Land surface temperature and emissivity estimation from passive sensor data: Theory and practice-current trends. *International Journal of Remote sensing,* 23**,** 2563-2594.

Defries, R. S., Foley, J. A. & Asner, G. P. 2004. Land- use choices: Balancing human needs and ecosystem function. *Frontiers in Ecology and the Environment,* 2**,** 249-257.

Di Gregorio, A. & Jansen, L. J. 2000. Land cover classification system (LCCS): classification concepts and user manual for software version 1.0.

Dong, F., Chen, J. & Yang, F. A Study of Land Surface Temperature Retrieval and Thermal Environment Distribution Based on Landsat-8 in Jinan City. IOP Conference Series: Earth and Environmental Science, 2018. IOP Publishing, 042008.

Du, C., Ren, H., Qin, Q., Meng, J. & Li, J. Split-window algorithm for estimating land surface temperature from Landsat 8 TIRS data. 2014 IEEE Geoscience and Remote Sensing Symposium, 2014. IEEE, 3578-3581.

Eckert, S., Kiteme, B., Njuguna, E. & Zaehringer, J. G. 2017. Agricultural expansion and intensification in the foothills of Mount Kenya: a landscape perspective. *Remote Sensing of Environment,* 9**,** 784.

Fao, U. 1999. Terminology for integrated resources planning and management. *Food and Agriculture Organization/United Nations Environmental Programme, Rome, Italy/Nairobi, Kenia*.

Foody, G. M. 2002. Status of land cover classification accuracy assessment. *Remote sensing of environment,* 80**,** 185-201.

Galeon, F. 2009. Estimation of the population in informal settlement communities using a high-resolution satellite image.

Gao, J. 2009. *Digital Analysis of Remotely Sensed Imagery: Multi-Temporal Image Analysis*, The McGraw-Hill Companies.

Gashaw, T., Bantider, A. & Mahari, A. 2014. Evaluations of land use/land cover changes and land degradation in Dera District, Ethiopia: GIS and remote sensing-based analysis. *International Journal of Scientific Research in Environmental Sciences,* 2**,** 199.

Gebrekidan, W. Modeling land surface temperature from satellite data, the case of Addis Ababa. Proceedings of the United Nations Conference Centre Addis Ababa, 2016. 23-24.

Guo, W., Ni. X., Jin, D., and Shuheng, L. 2014. Spatial-temporal patterns of vegetation dynamics and their relationships to climate variations in Qinghai Lake Basin using MODIS time-series data. *Journal of Geographical Sciences,* 2014, 24(6):1009-1021.

Hansen, M. C., Potapov, P. V., Moore, R., Hancher, M., Turubanova, S. A., Tyukavina, A., Thau, D., Stehman, S., Goetz, S. J. & Loveland, T. R. 2013. High-resolution global maps of 21st-century forest cover change. *science,* 342**,** 850-853.

Houghton, R.A., 1994. The worldwide extent of land-use change. BioScience, 44(5), pp.305-313

Hurni, H., Tato, K. & Zeleke, G. 2005. The implications of changes in population, land use, and land management for surface runoff in the upper Nile basin area of Ethiopia. *Mountain Research Development,* 25**,** 147-154.

Jensen, J. R. 1996. *Introductory digital image processing: a remote sensing perspective*, Prentice-Hall Inc.

Jensen, J. R. 2015. Introductory Digital Image Processing: A Remote Sensing Perspective.

Jiménez-Muñoz, J. C., Sobrino, J. A., Skoković, D., Mattar, C. & Cristóbal, J. 2014. Land surface temperature retrieval methods from Landsat-8 thermal infrared sensor data. *IEEE Geoscience and remote sensing letters,* 11**,** 1840-1843.

Jin, M., Li, J., Wang, C. & Shang, R. 2015. A practical split-window algorithm for retrieving land surface temperature from Landsat-8 data and a case study of an urban area in China. *Remote sensing* 7**,** 4371-4390.

Kalma, J. D., Mcvicar, T. R. & Mccabe, M. F. 2008. Estimating land surface evaporation: A review of methods using remotely sensed surface temperature data. *Surveys in Geophysics,* 29**,** 421-469.

Kayet, N., Pathak, K., Chakrabarty, A. & Sahoo, S. 2016. Spatial impact of land use/land cover change on surface temperature distribution in Saranda Forest, Jharkhand. *Modeling Earth Systems Environment,* 2**,** 127.

Kustas, W. & Anderson, M. 2009. Advances in thermal infrared remote sensing for land surface modeling. 149**,** 2071-2081.

Lakshmi Kumar, T., Koteswara Rao, K., Barbosa, H. & Prabha Jothi, E. 2013. Studies on the spatial pattern of NDVI over India and its relationship with rainfall, air temperature, soil moisture adequacy, and ENSO. *Geofizika,* 30**,** 1-18.

Lambin, E. F., Geist, H. J. & Lepers, E. 2003. Dynamics of land-use and land-cover change in tropical regions. *Annual review of environment resources,* 28**,** 205-241.

Lambin, E. F. & Meyfroidt, P. 2011. Global land-use change, economic globalization, and the looming land scarcity. *Proceedings of the National Academy of Sciences,* 108**,** 3465-3472.

Lambin, E. F., Turner, B. L., Geist, H. J., Agbola, S. B., Angelsen, A., Bruce, J. W., Coomes, O. T., DiRzo, R., Fischer, G. & Folke, C. 2001. The causes of land-use and land-cover change: moving beyond the myths. *Global environmental change,* 11**,** 261-269.

Lamchin, M., Park, T., Lee, J.-Y. & Lee, W.-K. 2015. Monitoring of vegetation dynamics in Mongolia using MODIS NDVIs and their relationship to rainfall by natural zone. *Journal of the Indian Society of Remote Sensing,* 43**,** 325-337.

Lamson-Hall, P., Degroot, D., Martin, R., Tafesse, T. & ANGEL, S. 2015. A New Plan for African Cities: The Ethiopia Urban Expansion Initiative.

Lazzarini, M., Marpu, P. R. & Ghedira, H. 2013. Temperature-land cover interactions: The inversion of urban heat island phenomenon in desert city areas. *Remote Sensing of Environment,* 130**,** 136-152.

Lemlem, A. 2007. *Assessing the impact of land use and land cover change on groundwater recharge using Rs and Gis; a case of Awassa catchment, Southern Ethiopia.* M. Sc. Thesis. Addis Ababa University, Ethiopia.

LI, J., Lewis, J., Rowland, J., Tappan, G. & Tieszen, L. 2004. Evaluation of land performance in Senegal using multi-temporal NDVI and rainfall series. *Journal of Arid Environments,* 59**,** 463-480.

Li, Z.-L., Tang, B.-H., Wu, H., Ren, H., Yan, G., Wan, Z., Trigo, I. F. & Sobrino, J. A. 2013. Satellite-derived land surface temperature: Current status and perspectives. *Remote Sensing of Environment***,** 14-37.

Lillesand, T., Kiefer, R. & Chipman, J. 2004. Remote sensing and image interpretation. *Remote sensing and image interpretation.*

Lillesand, T., Kiefer, R. & Chipman, J. J. R. S. 2008. Digital image interpretation and analysis. *Remote sensing and image interpretation,* 6**,** 545-81.

Lu, D. & Weng, Q. 2007. A survey of image classification methods and techniques for improving classification performance. *International Journal of Remote sensing,* 28**,** 823-870.

Maitima, J. M., Mugatha, S. M., Reid, R. S., Gachimbi, L. N., Majule, A., Lyaruu, H., Pomery, D., Mathai, S. & Mugisha, S. 2009. The linkages between land-use change, land degradation, and biodiversity across East Africa. *African Journal of Environmental Science Technology,* 3.

Malik, M.S., Shukla, J.P., and Mishra, S., 2019. Relationship of LST, NDBI, and NDVI using Landsat-8 data in Kandaihimmat Watershed, Hoshangabad, India. *Indian Journal of Geo-Marine Sciences,* 48(01), pp.25-31.

Markham, B. & Barker 1986. Landsat MSS and TM post-calibration dynamic ranges, exoatmospheric reflectances, and at-satellite temperatures. EOSAT Landsat Tech. *Notes,* 1.

Mather, A. & Needle, C. 2000. The relationships between population and forest trends. *Geographical Journal,* 166**,** 2-13.

Mengistu, A. 2008. Climate variability and change. *Ethiopian journal of Animal production,* 8**,** 94-98.

Meyer, W. B. & Turner, B. L. 1992. Human population growth and global land-use/cover change. *Annual review of ecology and systematics,* 23**,** 39-61.

Niamir-Fuller, M., Kerven, C., Reid, R. & Milner-Gulland, E. 2012. Co-existence of wildlife and pastoralism on extensive rangelands: competition or compatibility? : SpringerOpen.

Pomeroy, D., Tukahirwa, J., Mugisha, S., Nanyunja, R., Namaganda, M. & Chelimo, N. 2003. *Linkages between changes in land use, land degradation, and biodiversity in SW Uganda,* LUCID Project, International Livestock Research Institute.

Prata, A., Caselles, V., Coll, C., Sobrino, J. & Ottle, C. 1995. Thermal remote sensing of land surface temperature from satellites: Current status and prospects. *Remote Sensing Reviews,* 12**,** 175-224.

Price, J. C. 1984. Land surface temperature measurements from the split window channels of the NOAA 7 Advanced Very High-Resolution Radiometer. *Journal of Geophysical Research: Atmospheres,* 89**,** 7231-7237.

Qijiao, X. and Zhixiang, Z. (2015). Impact of urbanization on urban heat island effect based on

TM imagery in Wuhan, China. *Environ. Eng. Manag. J.* 14: 647–655.

Qin, Z., Dall'olmo, G., KarnielI, A. & Berliner, P. 2001. Derivation of the split-window algorithm and its sensitivity analysis for retrieving land surface temperature from NOAA- advanced very high-resolution radiometer data. *Journal of Geophysical Research: Atmospheres,* 106**,** 22655-22670.

Rinner, C. & Hussain, M. 2011. Toronto's urban heat island—Exploring the relationship between land use and surface temperature. *Remote Sensing,* 3**,** 1251-1265.

Rosenstein, O., Qin, Z., Derimian, Y. & Karnieli, A. 2014. Derivation of land surface temperature for Landsat-8 TIRS using a split window algorithm. *Sensors,* 14**,** 5768-5780.

Schmugge, T., Hook, S. & Coll, C. 1998. Recovering surface temperature and emissivity from thermal infrared multispectral data. *Remote Sensing of Environment,* 65**,** 121-131.

Small, C. 2004. Global population distribution and urban land use in geophysical parameter space. *Earth Interactions,* 8**,** 1-18.

Sisay, H., Teshome, S., and Demel, T. 2016. Land use and land cover change in the Bale

Mountain Eco-Region of Ethiopia from 1985 to 2015. *Land*, 5(4):41.

Sobrino, J., Jimenez-Munoz, J., El-Kharraz, J., Gómez, M., Romaguera, M. & Soria, G. 2004. Single-channel and two-channel methods for land surface temperature retrieval from

DAIS data and its application to the Barrax site. *International Journal of Remote Sensing,* 25**,** 215-230.

Sobrino, J., Jiménez-Muñoz, J., Zarco-Tejada, P., Sepulcre-Cantó, G., Miguel, E. D., Sòria, G., Romaguera, M., Julien, Y., Cuenca, J. & Hidalgo, V. 2009. Thermal remote sensing from Airborne Hyperspectral Scanner data in the framework of the SPARC and SEN2FLEX projects: an overview. *Hydrology Earth System Sciences,* 13**,** 2031-2037.

Sobrino, J., Raissouni, N. & LI, Z.-L. 2001. A comparative study of land surface emissivity retrieval from NOAA data. *Remote Sensing of Environment,* 75**,** 256-266.

Sun, Q., Wu, Z. & Tan, J. 2012. The relationship between land surface temperature and land use/land cover in Guangzhou, China. *Environmental Earth Sciences,* 65**,** 1687-1694.

Tempfli, K., Huurneman, G., Bakker, W., Janssen, L., Feringa, W., Gieske, A., Grabmaier, K., Hecker, C., Horn, J. & Kerle, N. 2009. *Principles of remote sensing: an introductory textbook,* International Institute for Geo-Information Science and Earth Observation.

Tran, T. V. & Ha, D. X. B. 2010. Study of the impact of urban development on surface temperature using remote sensing in Ho Chi Minh City, Northern Vietnam. *Geographical Research,* 48**,** 86-96.

United Nations (UN) 2014. *World Urbanization Prospects: The 2014 Revision-Highlights,* UN.

United States Geological Survey (USGS) in 2016. Landsat 8 (L8) data users handbook. Department of the Interior US Geological Survey, LSDS-.

United States Geological Survey (USGS), 2013. Using the USGS Landsat 8 product.

http://landsat.usgs.gov/Landsat8_Using_Product.php (29 Jun. 2015).

Voogt, J. A. & Oke, T. R. 2003. Thermal remote sensing of urban climates. *Remote sensing of environment,* 86**,** 370-384.

Wan, Z. 2013. Collection-6 MODIS Land Surface Temperature Products Users' Guide.

Wang, F., Qin, Z., Song, C., Tu, L., Karnieli, A. & Zhao, S. 2015. An improved mono-window algorithm for land surface temperature retrieval from Landsat 8 thermal infrared sensor data. *Remote sensing,* 7**,** 4268-4289.

Wei, H., Yongnian, Z. and Songnian, L. (2015). An analysis of urban expansion and its associated thermal characteristics using Landsat imagery. Geocarto Int. 30: 93–103.

Weng, Q. 2009. Thermal infrared remote sensing for urban climate and environmental studies: Methods, applications, and trends. *ISPRS Journal of Photogrammetry and Remote Sensing,* 64**,** 335-344.

Weng, Q. & Larson, R. C. 2005. Satellite remote sensing of urban heat islands: current practice and prospects. Geo-spatial technologies in urban environments. Springer.

Weng, Q., Lu, D. & Schubring, J. 2004. Estimation of land surface temperature–vegetation abundance relationship for urban heat island studies. *Remote sensing of Environment,* 89**,** 467-483.

Work, N. 2018. The impacts of vegetation cover change on rainfall and land surface

temperature using remote sensing: a case study of the North Gondar zone. M.Sc. Thesis Addis Ababa University, Ethiopia.

Xiong, Y., Huang, S., Chen, F., Ye, H., Wang, C. & Zhu, C. 2012. The impacts of rapid urbanization on the thermal environment: A remote sensing study of Guangzhou, South China. *Remote sensing,* 4**,** 2033-2056.

Xiuwan, C. 2002. Using remote sensing and GIS to analyze land cover change and its impacts on regional sustainable development. *International journal of remote sensing,* 23**,** 107-124.

Yang, L., Xian, G., Klaver, J. M. & Deal, B. 2003. Urban land-cover change detection through sub-pixel imperviousness mapping using remotely sensed data. *Photogrammetric Engineering and Remote Sensing,* 69**,** 1003-1010.

Yuan, F. & Bauer, M. E. 2007. Comparison of impervious surface area and normalized difference vegetation index as indicators of surface urban heat island effects in Landsat imagery. *Remote Sensing Of Environment,* 106**,** 375-386.

YUE, W., Xu, J., Tan, W. & Xu, L. 2007. The relationship between land surface temperature and NDVI with remote sensing: application to Shanghai Landsat 7 ETM+ data. *International Journal of Remote Sensing,* 28**,** 3205-3226.

Zha, Y., Gao, J. & Ni, S. 2003. Use of normalized difference built-up index in automatically mapping urban areas from TM imagery. *International journal of remote sensing,* 24**,** 583-594.

ZIENA, L. 2017. Mapping land use and land cover change and their effects on urban_ pre-urban agriculture in Debre Markos town. MSc. Thesis.Addis Ababa University, Ethiopia.

7. ANNEX

Annex 1: 2018 Landsat images with sample photographs that were used during image classification.

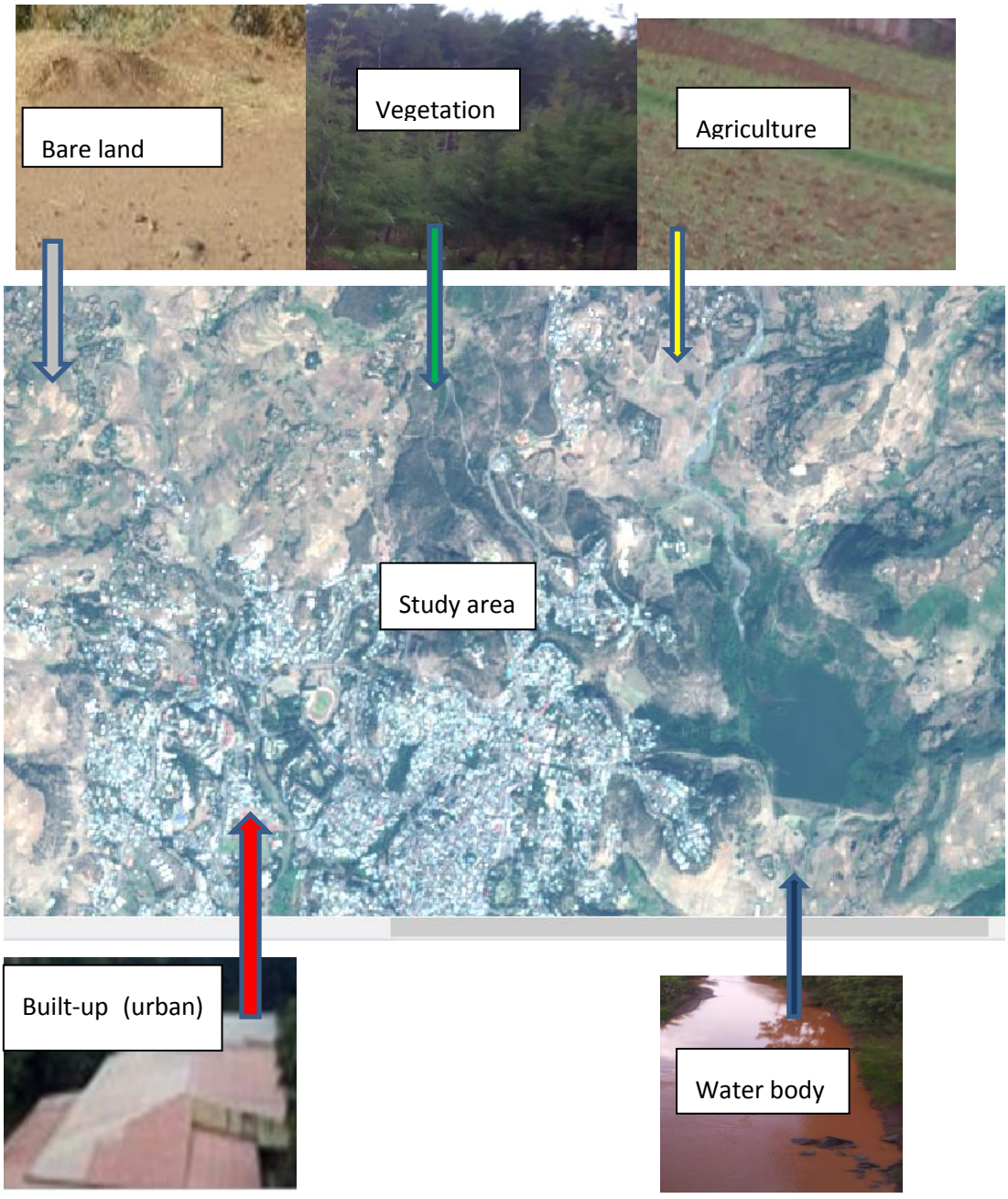

Annex 2: Ground points were used for accuracy assessment of LULC classification.

	2018		2002		1988	
FID	X	Y	X	Y	X	Y
1	333340.21	1393346.50	333732.25	1392363.88	333340.21	1393346.50
2	333522.28	1393380.06	333763.34	1392495.56	333435.61	1393310.54
3	333588.31	1393131.22	333524.21	1392220.50	333496.88	1393382.87
4	332043.59	1392799.22	332715.45	1392436.96	333522.28	1393380.06
5	331685.78	1392429.41	332490.98	1394086.79	333532.26	1393282.88
6	332204.66	1392288.85	332689.45	1395412.99	333498.91	1393247.23
7	332606.47	1392214.81	332715.71	1396128.79	329889.42	1384337.18
8	332550.50	1392509.06	332732.95	1396177.81	333190.30	1395320.12
9	330018.27	1383538.49	332669.76	1396165.68	332828.79	1395052.20
10	329982.41	1383705.08	332648.53	1396140.03	332615.84	1394774.13
11	329951.40	1383937.35	332653.41	1396231.37	332099.50	1394045.62
12	329928.63	1384074.55	332608.27	1396240.38	332158.87	1393870.26
13	329903.58	1384194.28	332647.21	1396359.29	332750.06	1393782.05
14	329874.92	1384420.56	332532.91	1396301.55	332769.64	1393544.87
15	333347.08	1395302.38	332713.49	1396286.11	331385.57	1393864.87
16	333190.30	1395320.12	332719.27	1396346.25	331450.64	1394174.78
17	333428.12	1395319.28	332825.80	1396466.87	332338.26	1394352.30
18	333580.29	1395089.73	332795.02	1396572.37	333723.17	1394663.66
19	333521.58	1395026.35	332669.15	1396524.76	333795.83	1394510.58
20	332828.79	1395052.20	332600.73	1396509.68	333636.82	1394425.66
21	332615.84	1394774.13	332795.78	1396665.84	333555.29	1394324.92
22	333038.26	1394681.49	332687.32	1396733.07	333393.25	1394354.96
23	331780.84	1393477.01	332742.87	1396756.20	333545.50	1394750.43
24	331582.75	1393602.63	332809.34	1396846.52	333689.59	1394773.49
25	332099.50	1394045.62	332649.44	1396941.15	334001.85	1394421.32
26	332750.06	1393782.05	332791.91	1397059.68	329096.91	1388321.11
27	332769.64	1393544.87	332952.05	1397006.19	332136.72	1395419.84
28	331655.33	1393253.63	333039.26	1397001.92	331636.66	1394829.82
29	331416.23	1392911.44	333040.22	1396998.26	330768.95	1385796.58
30	331385.57	1393864.87	333039.47	1396944.84	333290.73	1393612.16
31	331450.64	1394174.78	332987.97	1396906.97	333629.39	1393860.87
32	332844.47	1394151.53	332959.40	1396962.12	333460.06	1394178.37
33	333723.17	1394663.66	332875.79	1396876.99	334645.40	1392575.00
34	333721.75	1394419.97	333088.66	1396829.39	335174.56	1393135.91
35	333555.29	1394324.92	332814.16	1397186.43	335560.86	1394734.00
36	333352.39	1394557.53	332987.09	1397182.54	334957.61	1395189.08

37	333545.50	1394750.43	332902.97	1397343.55	335100.48	1395416.63
38	333792.30	1394780.63	332821.45	1397279.98	336645.65	1394728.71
39	334001.85	1394421.32	332786.20	1397252.42	334105.65	1401089.30
40	334104.63	1394775.82	332678.92	1397280.60	332856.81	1399216.05
41	332653.41	1396231.37	332714.10	1397314.79	332528.73	1400755.93
42	332713.49	1396286.11	332822.00	1397354.87	332856.81	1400475.47
43	332719.27	1396346.25	332743.12	1397372.15	332839.61	1394785.98
44	332669.15	1396524.76	332754.19	1397407.15	331674.78	1393565.80
45	332987.97	1396906.97	332906.04	1397440.55	331951.12	1393352.33
46	332754.19	1397407.15	332983.60	1397475.60	331655.33	1393253.63
47	334755.53	1392527.19	332977.18	1397473.87	331565.22	1394612.86
48	333843.87	1392479.93	332920.24	1397490.58	333244.27	1395056.07
49	333732.25	1392363.88	332847.53	1397485.58	333580.29	1395089.73
50	333763.34	1392495.56	333348.09	1394862.54	332767.10	1394611.29
51	330789.06	1387970.38	330542.10	1394319.55	334034.29	1398548.36
52	330677.89	1387768.26	330651.58	1394421.56	334015.90	1398562.51
53	330576.58	1382868.35	330685.57	1394400.67	333894.48	1398809.47
54	330048.39	1386532.45	330718.82	1394364.30	333744.36	1399070.53
55	333744.36	1399070.53	330735.16	1394354.69	333580.24	1399110.21
56	333642.51	1399225.89	330763.63	1394337.04	333642.51	1399225.89
57	333468.02	1399368.51	330861.54	1394358.14	333649.81	1399507.38
58	333649.81	1399507.38	330802.53	1394281.39	333020.10	1399564.51
59	334014.09	1399405.69	330793.39	1394242.84	332383.11	1399509.96
60	332846.75	1399493.74	330771.32	1394186.44	332338.30	1399427.37
61	332768.37	1395438.52	330785.61	1394158.48	330461.48	1382813.94
62	332752.77	1395465.61	330832.64	1394193.15	330722.05	1382819.82
63	332543.01	1395506.55	332509.44	1395525.89	330703.61	1382900.24
64	332462.59	1395522.51	332429.30	1395514.41	330552.71	1383041.18
65	331828.63	1395555.12	331817.79	1395596.01	330766.39	1383501.88
66	331797.59	1395762.06	331828.63	1395555.12	330681.67	1384396.55
67	335165.50	1394428.29	331892.18	1395498.33	330707.78	1384935.24
68	335164.94	1394368.66	331934.06	1395470.43	330873.70	1385297.77
69	335142.25	1394277.42	335165.50	1394428.29	330139.08	1385732.55
70	335101.91	1394215.71	335164.94	1394368.66	330392.78	1386234.94
71	335000.89	1394164.52	335142.25	1394277.42	330537.03	1386644.50
72	334975.60	1394168.10	335101.91	1394215.71	330365.93	1387317.88
73	334849.01	1394184.32	334849.01	1394184.32	330142.52	1388147.22
74	334711.40	1394304.36	334559.65	1396349.55	330415.25	1388654.59
75	333379.45	1395543.79	333378.21	1395609.07	330427.58	1388974.22
76	333316.79	1395548.59	333129.16	1396177.58	330578.38	1390014.29
77	333328.02	1395980.95	331297.77	1399723.91	330055.54	1389969.16

78	333347.77	1395939.79	331549.13	1399508.93	330447.86	1390562.10
79	333251.07	1395846.33	331572.28	1399244.35	330701.79	1390393.89
80	333216.89	1396020.54	332478.48	1399833.05	330449.34	1391141.65
81	334324.44	1387527.47	334240.28	1400264.98	334755.53	1392527.19
82	334318.23	1387524.51	333486.21	1399455.35	334293.14	1393001.12
83	334317.13	1387522.31	337605.78	1402352.55	334299.56	1393133.27
84	334575.68	1395068.67	332832.16	1401781.04	334152.23	1392853.92
85	334599.43	1395080.48	339166.30	1399034.66	334074.35	1392671.52
86	334715.79	1395116.97	329942.91	1397542.41	333950.15	1392408.29
87	334718.90	1395147.70	327625.15	1392589.40	333970.05	1392111.60
88	334723.49	1395171.13	331498.66	1392224.28	333708.26	1392161.58
89	334754.29	1395142.52	332832.16	1391398.77	332653.41	1396231.37
90	334809.62	1395129.04	330689.03	1387969.77	332795.02	1396572.37
91	334884.08	1395117.54	335408.29	1387404.96	332875.79	1396876.99
92	334937.03	1395105.62	335046.43	1387822.97	332822.00	1397354.87
93	335006.61	1395095.81	335016.60	1387511.97	332847.53	1397485.58
94	335125.07	1395102.10	335451.43	1387100.39	332698.44	1396646.28
95	335139.00	1395049.36	335735.96	1387844.12	332795.78	1396665.84
96	335055.50	1394925.84	339294.20	1398844.16	332687.32	1396733.07
97	335107.19	1394922.22	337305.85	1400657.89	333088.66	1396829.39
98	335160.46	1394909.08	326933.11	1381362.84	330576.58	1382868.35
99	335201.01	1394895.24	326668.52	1379153.57	330245.89	1383872.77
100	335149.52	1394728.05	325173.07	1388950.89	330792.95	1387966.26
101	335080.44	1394730.89	329096.91	1388321.11	334307.93	1387153.66
102	334356.43	1396505.82	329377.37	1388797.37	334310.63	1387149.77
103	334394.73	1396496.53	330025.07	1387843.81	334318.32	1387145.41
104	333469.51	1396155.45	329915.60	1390116.86	334324.71	1387142.61
105	333443.32	1396246.98	332136.72	1395419.84	334352.16	1387153.18
106	333463.34	1396288.57	331549.35	1395245.21	334910.50	1387412.35
107	333512.24	1396439.40	331636.66	1394829.82	334936.53	1387498.05
108	333365.91	1396088.47	331565.22	1394612.86	335347.02	1387389.93
109	333348.24	1395891.11	333950.89	1396000.16	335245.15	1387438.64
110	333335.18	1395830.35	333969.41	1395603.28	335160.87	1387541.67
111	333331.11	1395729.15	334477.41	1395082.05	335159.95	1387703.18
112	333227.94	1396088.95	333863.57	1395172.01	335046.43	1387822.97
113	333058.78	1396348.24	329610.08	1385955.33	335045.14	1387730.83
114	333050.61	1396399.62	329758.24	1384992.24	335043.12	1387607.28
115	333099.03	1396412.94	330768.95	1385796.58	335019.71	1387523.67
116	332480.00	1394252.12	329329.62	1386410.41	334969.32	1387435.80
117	332490.98	1394086.79	329038.57	1386870.79	334968.21	1387431.49
118	330244.08	1390684.11	327826.78	1387564.00	335406.18	1386866.35

119	330201.47	1390827.74	326080.53	1387018.96	330542.10	1394319.55
120	333379.45	1395543.79	324889.90	1386675.00	330685.57	1394400.67
121	330738.58	1384131.16	324598.86	1386548.00	330718.82	1394364.30
122	330576.86	1384242.51	333307.42	1393109.85	330798.30	1394319.25
123	330549.66	1384330.95	332550.50	1392509.06	330802.53	1394281.39
124	330718.09	1384287.15	332769.64	1393544.87	330785.61	1394158.48
125	330681.67	1384396.55	333865.44	1394412.16	332462.59	1395522.51
126	330498.69	1384459.13	333496.88	1393382.87	332429.30	1395514.41
127	330445.51	1384528.37	333588.31	1393131.22	332402.97	1395489.46
128	330502.70	1384679.36	333385.32	1393089.59	331817.79	1395596.01
129	330661.20	1384610.50	332001.65	1392595.81	331828.63	1395555.12
130	330729.53	1384789.42	331685.78	1392429.41	331892.18	1395498.33
131	334040.48	1398547.99	330047.81	1383386.98	331934.06	1395470.43
132	334034.29	1398548.36	329874.92	1384420.56	335240.12	1394856.29
133	334030.28	1398550.59	332839.61	1394785.98	335164.94	1394368.66
134	334015.90	1398562.51	333002.37	1394749.07	335142.25	1394277.42
135	333855.05	1398717.11	333347.08	1395302.38	334913.67	1394148.76
136	333894.48	1398809.47	332828.79	1395052.20	330211.29	1382983.34
137	333799.58	1398854.05	331780.84	1393477.01	329935.55	1384417.33
138	333650.41	1398960.68	331674.78	1393565.80	331498.66	1392224.28
139	333580.24	1399110.21	332099.50	1394045.62	332832.16	1391398.77
140	333140.23	1399229.28	332158.87	1393870.26	330689.03	1387969.77
141	333033.20	1399225.59	331986.36	1393321.59	334499.47	1396330.54
142	332774.40	1399291.72	331655.33	1393253.63	334604.15	1396378.49
143	330552.71	1383041.18	331416.23	1392911.44	334611.28	1396427.23
144	330509.10	1383220.98	331385.57	1393864.87	334604.01	1396485.24
145	330734.64	1383259.03	331450.64	1394174.78	334549.03	1396484.90
146	330689.71	1383289.16	332338.26	1394352.30	334514.16	1396466.85
147	330530.17	1383439.77	333555.29	1394324.92	334462.06	1396455.76
148	330766.39	1383501.88	333527.50	1394887.16	334472.36	1396339.65
149	330345.63	1383902.61	334001.85	1394421.32	334473.11	1396337.99
150	333378.21	1395609.07	334104.63	1394775.82	334473.53	1396335.55
151	333242.00	1396133.45	335717.77	1395267.04	332147.68	1395769.62
152	333243.62	1396205.67	335731.52	1395142.16	332260.40	1395871.28
153	333222.22	1396244.29	335639.45	1395075.48	332443.93	1395303.92
154	333316.79	1395548.59	335567.48	1395148.51	331971.30	1395300.07
155	333328.02	1395980.95	335658.50	1395213.07	332669.35	1394451.46
156	333347.77	1395939.79	335644.74	1395299.85	332972.98	1394481.21
157	335101.91	1394215.71	335693.42	1395359.12	333030.27	1394560.19
158	330618.01	1394403.95	335521.97	1395213.07	333061.86	1394593.19
159	330651.58	1394421.56	335637.33	1395149.57	333119.16	1394656.13

160	332490.98	1394086.79	335741.05	1395052.20	333264.58	1394776.85
161	335717.77	1395267.04	335825.72	1395153.80	333399.92	1396942.83
162	335731.52	1395142.16	335832.07	1395258.58	333237.31	1396964.25
163	335639.45	1395075.48	335772.80	1395254.34	333392.06	1397178.06
164	335567.48	1395148.51	335771.74	1395339.01	333390.41	1397303.08
165	335658.50	1395213.07	335671.20	1395432.14	333811.22	1397834.26
166	335644.74	1395299.85	335654.27	1395390.87	334654.13	1395799.20
167	335693.42	1395359.12	335580.18	1395289.27	334346.62	1395734.29
168	335521.97	1395213.07	335517.74	1395258.58	334236.66	1395713.69
169	335637.33	1395149.57	335475.41	1395196.13	333956.59	1395715.32
170	335741.05	1395052.20	335499.75	1395086.07	334560.56	1394859.24
171	335825.72	1395153.80	335598.17	1394972.83	334197.57	1394597.29
172	335832.07	1395258.58	335664.85	1394923.08	334863.52	1394513.11
173	335772.80	1395254.34	335697.66	1394988.70	334807.69	1394647.29
174	335771.74	1395339.01	335595.00	1395028.92	334984.72	1394749.25
175	335671.20	1395432.14	335534.67	1395115.70	333597.98	1383802.83
176	335654.27	1395390.87	335485.99	1395160.15	333299.91	1384750.04
177	335580.18	1395289.27	335717.77	1395213.07	330621.25	1393469.16
178	335517.74	1395258.58	335783.38	1395160.15	330591.78	1392989.11
179	335475.41	1395196.13	335803.49	1395105.12	331107.91	1392367.22
180	335499.75	1395086.07	335676.49	1395089.24	330114.81	1391769.11
181	335598.17	1394972.83	335549.58	335549.58	337852.19	1401082.19
182	335485.99	1395160.15	335759.26	335759.26	331481.86	1402356.26
183	335717.77	1395213.07	335755.95	335755.95	339629.18	1397964.08
184	335783.38	1395160.15	335480.12	335480.12	335874.04	1396270.92
185	335803.49	1395105.12	335449.70	335449.70	337500.15	1398081.43
186	335676.49	1395089.24	335883.61	335883.61	329587.53	1401518.06
187	335549.58	335549.58	335908.75	335908.75	327961.41	1391090.83
188	335759.26	335759.26	335644.17	335644.17	332923.57	1382256.18
189	335755.95	335755.95	335262.12	1395580.08	338321.59	1399808.13
190	335480.12	335480.12	335284.95	1395469.99	336070.87	1393408.00
191	335449.70	335449.70	335400.53	1395391.99	333388.85	1396851.41
192	335883.61	335883.61	335570.20	1395198.31	331965.21	1395797.14
193	335908.75	335908.75	335713.09	1394919.71	334237.00	1396443.79
194	335644.17	335644.17	335192.95	1395723.34	330103.77	1391447.81
195	333316.79	1395548.59	335222.05	1395609.57	335639.34	1399355.50
196	333328.02	1395980.95	335399.32	1395681.00	325719.02	1381270.22
197	333347.77	1395939.79	335547.49	1395487.86	332637.66	1393431.42
198	335164.94	1394368.66	335568.66	1394773.48	336815.01	1388695.10
199	335142.25	1394277.42	335462.82	1395781.55	334221.40	1394307.38
200	333348.24	1395891.11	335367.57	1395016.90	334194.41	1394497.88

201	331646.34	1401331.71	335468.62	1392860.71	332679.39	1394771.85
202	336295.06	1401331.71	334745.49	1391362.79	334383.92	1395649.94
203	338361.15	1398749.09	335107.05	1389658.26	336811.58	1395649.94
204	339962.38	1398439.17	335468.62	1388108.69	333557.48	1398594.13
205	339755.77	1395856.55	334228.96	1387592.17	332524.43	1386765.73
206	338722.72	1394100.37	333247.57	1386817.38	331904.60	1385577.72
207	337431.41	1392860.71	333040.96	1385112.85	330923.21	1384493.02
208	336346.71	1391672.71	333867.39	1382995.10	328960.41	1383718.24
209	336036.80	1390433.05	333815.74	1381910.40	328805.46	1382013.71
210	336553.32	1389038.44	332266.17	1382995.10	326687.71	1383098.41
211	336295.06	1387488.86	329786.85	1383150.06	326791.01	1380825.70
212	334900.44	1386404.16	327927.37	1381600.49	324673.26	1387643.82
213	334228.96	1385112.85	327669.10	1383614.93	324673.26	1390071.48
214	334952.09	1383614.93	326997.62	1385164.50	332782.69	1383873.19
215	335313.66	1381497.18	325861.27	1386610.77	333505.83	1388418.61
216	335003.75	1379895.96	325551.36	1388212.00	331852.95	1389141.74
217	333350.87	1380670.74	326326.14	1389296.70	328650.50	1391259.49
218	331852.95	1381600.49	327824.06	1390226.44	329941.81	1393738.80
219	330923.21	1381600.49	329270.33	1392085.93	331801.30	1391879.32
220	330045.12	1380929.01	330613.29	1394152.02	333815.74	1389813.22
221	329786.85	1379482.74	331491.38	1396063.16	330923.21	1395030.11
222	327979.02	1380205.87	332111.21	1398180.91	332317.82	1396786.30
223	326997.62	1378139.78	334745.49	1398594.13	338980.98	1395133.42
224	327462.49	1376745.16	336553.32	1396992.91	338051.24	1397147.86
225	326687.71	1376693.51	335210.36	1395030.11	335985.14	1398129.26
226	326067.88	1379947.61	332886.00	1392240.88	333660.78	1397251.17
227	325603.01	1382220.32	330923.21	1388780.17	330561.64	1397819.35
228	325603.01	1384596.33	327410.84	1386610.77	333299.22	1399472.22
229	324518.31	1385267.81	329218.68	1389451.65	335985.14	1399110.66
230	323743.52	1387075.64	331749.65	1393325.59	335158.70	1400970.14
231	323588.56	1389090.09	333247.57	1396579.69	332989.30	1401435.01
232	323072.04	1390536.36	334900.44	1396631.34	337328.11	1399213.96
233	325448.05	1390742.96	333919.05	1393738.80	339032.64	1396218.12
234	326842.67	1391259.49	333040.96	1389296.70	337792.98	1394513.59
235	327669.10	1392395.84	331233.12	1386145.90	335107.05	1393893.76
236	328650.50	1393687.15	329218.68	1386920.69	333660.78	1394875.16
237	329528.59	1395340.03	327824.06	1388625.22	332731.04	1395959.86
238	330561.64	1396889.60	331956.25	1390484.70	332782.69	1393635.50
239	331078.16	1399213.96	330664.94	1392189.23	332834.35	1390278.09
240	329373.63	1400866.84	330355.03	1390742.96	330613.29	1389451.65
241	330613.29	1400556.92	331956.25	1387902.08	329321.98	1390433.05

242	332524.43	1400092.05	329321.98	1384957.89	335985.14	1395030.11
243	333867.39	1401331.71	331594.69	1383769.89	335881.84	1396218.12
244	334383.92	1399988.75	330509.99	1385371.11	335416.97	1397664.39
245	336295.06	1399833.79	327927.37	1385267.81	334280.61	1397871.00
246	337534.72	1400195.36	328547.20	1387592.17	332627.74	1397457.78
247	337276.45	1398180.91	326687.71	1387592.17	331388.08	1397251.17
248	339032.64	1397457.78	329890.16	1388263.65	329735.20	1396476.38
249	337792.98	1395959.86	333557.48	1391156.18	335210.36	1399885.44
250	336501.67	1394152.02	334177.31	1392344.19	333350.87	1400763.53

Annex 3: Error matrix of LULC classification of the study area in 1988.

1988		Reference Data							
		VEG	WB	AGR	BL	BU	Total	UA	Coerr
Classified Data	VEG	**42**		1			43	97.67	0.02
	WB		**48**				48	100.00	0
	AGR	7		**46**	7	1	61	75.41	0.24
	BL		2	3	**40**	3	48	83.33	0.12
	BU	1			3	**46**	50	92.00	0.08
Total		50	50	50	50	50	250		
PA (%)		84.00	96.00	92.00	80.00	92.00		OA=88.8%	
Omerr		0.16	0.04	0.08	0.20	0.08		K=86%	

Where; PA-producer accuracy, UA-user accuracy, OA- overall accuracy, k-kappa coefficient, Coerr-commission error, and Omerr-omission error.

Annex 4: Error matrix of LULC classification of the study area in 2002.

2002		Reference Data							
		VEG	WB	AGR	BL	BU	Total	UA	Coerr
Classified Data	VEG	**46**		1		1	48	95.83	0.04
	WB		**47**				47	100.00	0
	AGR	3		**45**	3	2	53	84.91	0.15
	BL		3	3	**44**	1	51	86.27	0.13
	BU	1		1	3	**46**	51	90.20	0.09
Total		50	50	50	50	50	250		
PA (%)		92.00	94.00	90.00	88.00	92.00		OA=91.2%	
Omerr		0.08	0.06	0.10	0.12	0.08		K=89%	

Where; PA-producer accuracy, UA-user accuracy, OA- overall accuracy, k-kappa coefficient, Coerr-commission error, and Omerr-omission error.

Annex 5: Error matrix of LULC classification of the study area in 2018.

2018		Reference Data							
		VEG	WB	AGR	BL	BU	Total	UA	Coerr
Classified Data	VEG	**47**	1	2			50	94.00	0.06
	WB		**46**				46	100.00	0
	AGR	2	1	**45**	7	1	56	80.36	0.19
	BL	1	2	2	**42**		47	89.36	0.11
	BU			1	1	**49**	51	96.08	0.03
Total		50	50	50	50	50	250		
PA (%)		94.00	92.00	90.00	84.00	98.00		OA=91.6%	
Omerr		0.06	0.08	0.1	0.16	0.02		K=89.5%	

Where; PA-producer accuracy, UA-user accuracy, OA- overall accuracy, k-kappa coefficient, Coerr-commission error, and Omerr-omission error.

Annex 6: The conditional statement used to calculate LSE based on NDVI.

The calculation of land surface emissivity is based on NDVI using a raster calculator in ArcGIS by the following conditional statement provided below.

Con ("ndvi.tiff<0, 0.995, con ((ndvi.tiff>=0) & ("ndvi.tiff"<0.2), 0.974, con (("ndvi.tiff">=0.2) & (ndvi.tiff<0.5), Ev *pv +Es (1-pv) +(1-Es)*(1-Ev)*F*Ev, con(ndvi.tiff.>=0.5,0.986)))).

Where; EV-emissivity of vegetation (0.986), PV-proportional of vegetation, and Es (0.974)-emissivity of soil for band six for land sat five.

Con ("ndvi.tiff<0, 0.996, con ((ndvi.tiff>=0) & ("ndvi.tiff"<0.2), 0.973, con (("ndvi.tiff">=0.2) & (ndvi.tiff<0.5), Ev *pv +Es (1-pv) + (1-Es)*(1-Ev)*F*Ev, con (ndvi.tiff.>=0.5, 0.984)))).

Where; EV-emissivity of vegetation (0.984), PV- proportional of vegetation, and Es - emissivity of soil (0.973) for band ten for land sat eight.

Con ("ndvi.tiff<0, 0.984, con ((ndvi.tiff>=0) & ("ndvi.tiff"<0.2), 0.97, con (("ndvi.tiff">=0.2) & (ndvi.tiff<0.5), Ev *pv +Es (1-pv) + (1-Es)*(1-Ev)*F*Ev, con(ndvi.tiff.>=0.5,0.980)))).

Where; EV-emissivity of vegetation (0.980), PV- proportional of vegetation, and Es - emissivity of soil (0.970) for band eleven for land sat eight.

Declaration

I declare that this thesis entitled **"Assessment of Land Use and Land Cover Changes and its Impact on LST using remotely sensed data: In and Around Gondar Town, Ethiopia"** is my original work and has not been presented for a degree in any other university and that all sources of materials used for this thesis have been interestingly acknowledged.

Frew Fentahun Enyew Signature _____ Date ____/____/_____

School of Civil and Environmental Engineering

Addis Ababa University

This is certified that the thesis entitled "**Assessment of Land Use and Land Cover Changes and its Impact on LST using remotely sensed data: In and Around Gondar Town, Ethiopia**" is the original work of **Mr. Frew Fentahun Enyew** for the partial fulfillment of the Degree of Masters of Science in Geodesy and Geomatics (specialized in Geomatics) from Addis Ababa University under my guidance and supervision.

Dr. Ermias Teferi Signature _____ Date ____/____/____

Addis Ababa University